# Modifying Charge Carrier Injection Using Self-Assembled Monolayers in Organic Field-Effect Transistors

**Fatemeh Gholamrezaie**

University of Groningen
**Zernike Institute**
**for Advanced Materials**

# Modifying Charge Carrier Injection Using Self-Assembled Monolayers in Organic Field-Effect Transistors

**Fatemeh Gholamrezaie**

**Supervisor:** Dr. Bert de Boer and Kamal Asadi
**Group leader:** Prof. dr. ir. Paul W. M. Blom
**Referent:** Prof. dr. ir. Paul H. M. van Loosdrecht
**Period:** September 2006 – August 2007

**Molecular Electronics - Physics of Organic Semiconductors**
**Zernike Institute for Advanced Materials**
**Faculty of Mathematics and Natural Sciences**
**University of Groningen, The Netherlands**

# Table of Contents

**Table of Contents** **4**

**Perspective** **7**
Transistors in a century of electronics 7
Field-effect transistors (FET) 8
Organic field-effect transistors 8

Chapter 1 **Theory** **11**
1.1 Organic Semiconductors 11
1.1.1 The Basics 11
1.1.2 Small Molecule Organic Semiconductors 12
1.1.3 Semiconducting Polymers 13
1.2 Charge Transport in Organic Semiconductors 14
1.2.1 Charge Carriers in Conjugated Polymers 15
1.2.2 Hopping Transport 16
1.2.3 Multiple Trapping and Release Model 16
1.3 Applications of Semiconducting Polymers in Molecular Electronic Devices 17
1.3.1 Organic Field Effect Transistors; The Basics 17
1.3.2 Mobility 19
1.3.3 Contact Resistance and Injection 21
1.3.4 Transfer Line Method 25
1.3.5 Interface 27
1.4 Self-Assembly in the electronic devices 27
1.4.1 The Self-Assembly Technique 29
1.4.2 Work Function Change Induced by the Adsorbates 31
1.4.3 Tuning the Work Function by SAMs 31
1.4.4 Charge transport in Self-Assembled Monolayer 33
1.4.5 Applications of the SAMs on gate insulator 34

Chapter 2 **35**

**Experiments (Part 1)** **35**
2.1 SAM preparation 36
2.2 Spin-Coating 36
2.3 Electrical measurements 37
2.4 Results and Discussion (Part 1) 37
  2.4.1 MEH-PPV 37
  2.4.2 rr-P3HT 44

Chapter 3 **Experiment (Part 2)** **51**
3.1 Photolithography 51
3.2 Thermal Evaporation 52
3.3 Results and Discussion (Part 2) 54

**Conclusion** **63**

**Out Look** **65**

**Acknowledgment** **67**

**References** **68**

# Perspective

### Transistors in a century of electronics

In 1947, John Bardeen and Walter Brattain working at Bell Telephone Laboratories were trying to understand the nature of the electrons at the interface between a metal and a semiconductor. They found out that by making two point contacts very close to one another, they could make a three terminal device- the first “point contact” transistor.[1] They received the Nobel Prize in Physics, 1956, together with William Shockley, for their researches on semiconductor and their discovery of the transistor effect. A transistor is a semiconductor device, commonly used as an amplifier or an electrically controlled switch, which can be controlled by another electrical switch. By using many switches that control each other, we can built up very complicated logic circuits. The logic circuits can be built on a silicon chip with 1,000,000 transistors per square centimeters, with which this circuitry operates our computers, cellular phones, and all other modern electronics.

Electronic technology has rapidly improved in the past decades. The emphasis is to make better, cheaper faster and smaller electronic devices for application in modern life. In some of the most advanced chips used in a computer, several hundreds of millions of transistors are present. To be able to fit that many transistors, extremely small feature sizes are needed. In fact, today's transistors are many, many times smaller than even a single human hair. However, there is a practical size limitation, if the size is decreased further, it can affect their performance. Molecular electronics, which is a term that refers both to the use of molecular materials in electronics and electronics at molecular level, is an approach to pass this limit. The name originates form the fact that it uses molecules to function as switches and wires.[1]

**Field-effect transistors (FET)**

A field-effect transistor (FET) is a device that relies on the modulation of the conductance of a “channel” in the semiconductor by application of an electric field perpendicular to it. The principle of the field-effect transistor (FET) was first proposed by Lilienfeld in 1930.[2] It was only in 1960 that Kahng and Atalla fabricated the first silicon-based metal-oxide-semiconductor FET (MOSFET).[3] Nowadays, the MOSFET is probably the most component of modern microelectronics, both as discrete devices and in integrated circuits.[4]

**Organic field-effect transistors**

MOSFETs are mainly fabricated with single-crystalline silicon, because of the excellent quality of the silicon-silicon oxide interface. Although the first description of the field-effect in organic semiconductors dates back to 1970, Koezuka, in 1987,[5] reported a FET based on a conjugated polymer (polythiophene), which has the potential to be used as an electronic device.[4]

Among organic materials, conjugated polymers have attracted most attention for possible applications in molecular electronic devices because of their unique properties that provide the opportunity to produce low cost devices on large area plastic substrates and opening a new market segment. However, the precise control of all electrical properties of the electronic components is required.[6] Conjugated polymers are intrinsically semiconducting materials. They lack intrinsic mobile charges, but are able to transport charge generated by light, injected by electrodes, or provided by chemical dopants. It is the nature of the bonds between the carbon atoms, as will be described, that gives the conjugated polymers its interesting physical and chemical properties. In recent years, great advancements have been achieved in organic materials science for development of the devices such as organic light-emitting diodes (OLEDs), solar cells, electro-chemical cells, organic memories and organic field-effect transistors (OFETs).The interest for OFETs has drastically increased over the past few years,

and they have been extensively studied for many applications such as displays, identification tags and sensors. The stability and performance of OFETs depend on the preparation methods, diffusion of metal atoms, reactivity of the metal and organic materials, and roughness of the metallic contacts.[8]
Field-effect transistors require an Ohmic source and drain contacts for ideal operation. However, in many real situations, specifically in organic devices, the injection of charge carriers from metals into semiconductors can be an inefficient process that is non-Ohmic which has an adverse impact on the performance of transistors.[7] Improved charge injection for an enhanced device performance and tuning the work function of the metal to match the HOMO (or valance band) and/or LUMO (conduction band) is desirable. The performances of all the above-mentioned devices are determined by the work functions of their metal electrodes.[8]
The aim of this project is to improve or selectively block the injection of the charge carriers into the organic semiconductor by introducing a self-assembled monolayer on the contacts in several FET geometries. Tuning the work function of the metal electrodes in organic devices such as polymer light-emitting diode and photovoltaic cells was reported.[8] For the diode geometries the effect of the electrode modification is obvious. One can block the injection of holes or electrons. In three terminal devices, however, this effect is less clear since high gating potentials result in a highly electrostatic-doped semiconductor, which can give rise to strong band bending at the electrode/ polymer interface.

Thus, in this report, after briefly introducing the theory of organic semiconductors, the operation principles of the OFETs and the self-assembly technique, we present the result of tuning the work function of the contacts in the experimental parts. We will discuss the modification of the source and drain contacts in field-effect transistors using mainly two thiol-based molecules with apposing dipole moments as SAMs:

1. hexadecanethiol, $C_{16}H_{33}$-SH, to reduce the work function
2. perfluorinated decanethiol, $CF_3(CF_2)_7(CH_2)_2$-SH, to raise the work function

We will also use two different metals as source and drain electrodes:

1. gold

2. silver

and utilize this in two different geometries namely:

1. bottom-contact/ bottom-gate (BC/BG)
2. bottom-contact/ top-gate (BC/TG)

Furthermore, we will apply 3 different semiconducting polymers:

1. poly(2-methoxy-5-(2'-ethylhexyloxy)-1,4-phenylenevinylene) (MEH-PPV),
2. poly(3-hexyl thiophene) (rr- P3HT)
3. poly(9,9-dioctylfluorene) (PFO)

# Chapter 1
# Theory

## 1.1 Organic Semiconductors

Conjugated polymers have attracted great attention for electronics applications as they have many advantages over their inorganic counterparts, due to their unique mechanical properties. The electronic conduction in these materials has two requirements: (1) a continuous system of a large number of strongly interacting atomic orbital leading to the formation of electronic band structure, and (2) the presence of an insufficient number of charges to fill these bands.

### 1.1.1 The Basics

Organic Semiconductors are based on the unusual properties of the carbon atoms. Carbon, in the ground state, has four electrons in the outer electronic shell, 2 in *s* and 2 in *p* orbitals. The orbitals of these electrons may mix, under creation of four chemical bonds, to form four equivalent degenerate orbitals referred to as $sp^3$ hybrid orbitals in a tetrahedral orientation around the carbon atom. If only three chemical bonds are formed, they have three coplanar $sp^2$ hybridized orbitals which are at an angle of $120^o$ with each other. These bonds are called σ-bonds, and are associated with a highly localized electron density in the plane of the molecule. The energy difference between the occupied binding orbitals and the unoccupied anti-binding orbitals is quite large and well beyond the visible spectral range. Correspondingly, longer chains of bound carbon atoms would have a large gap between the highest occupied molecular orbital (σ-HOMO) (or σ) and the lowest unoccupied molecular orbital (σ-LUMO) (or σ*), leading to insulating properties. The one remaining free electron per carbon atom resides in the $p_z$ orbital, perpendicular to the plane

of the $sp^2$ hybridization. The $p_z$ orbitals on neighboring atoms overlap to form so-called π-bonds.[9]

Aliphatic molecules are singly bounded molecules like C-C or C-H that contain only sigma bonds, the positive charge of the nuclei prevents electron to travel along the axis of the molecule. Thus this structure can not easily transport electrons. Double bonds can be seen in the alkenes which contain double-carbon bonds, and referred to as unsaturated hydrocarbons. Ethene or ethylene is the simplest alkene, with the formula $C_2H_4$. Carbons with double bond are $sp^2$ hybridized, with 3 *sp* type hybrids available to form sigma bonds, and 1 *p* orbital with 1 electron for bonding. Thus these two adjacent *p* orbitals can overlap to form a *π*-bond shown in Figure 1.[10]

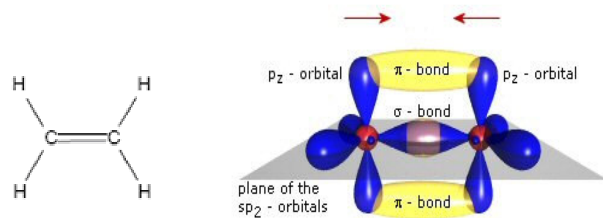


**Fig. 1** Schematic drawing of *σ*- and *π*-bonds in the Ethylene.

### 1.1.2 Small Molecule Organic Semiconductors

In contrast with the aliphatic molecule, there are molecules consists of alternating single and double bonds that link the subsequent atoms, $-\mathrm{C}=\mathrm{C}-$, and are called *conjugated* molecules. There is an extended series of overlapping *p* orbital which make the *π*-bond. In conjugated oligomers electrons from *π* are delocalize over entire molecule. These bonds have much smaller energetic difference between the *π*-HOMO and *π*-LUMO, compare to *σ* bond, leading to semiconducting properties.[9] This is shown in Figure 2. We can see delocalization, for instance in benzene ring ($C_6H_6$), as the basic unit, the π-bonds become delocalized and forms a *π* -system. The gap between occupied and empty states in this *π* -systems becomes smaller with increasing delocalization, leading to absorption and fluorescence in the visible part of the electromagnetic wave spectrum.

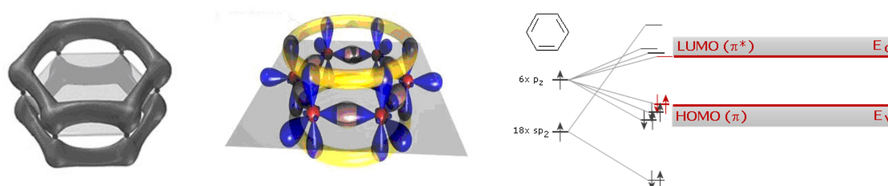


**Fig. 2** Scheme of a benzene ring and the energy structure. [11]

### 1.1.3 Semiconducting Polymers

The delocalization in benzene can be extended to other adjacent benzene rings. Poly(*p*-phenylene)- and poly(*p*-phenylene vinylene)-based molecules are good examples of conjugated polymers. Each carbon atom has one *p* orbital. Two adjacent *p* orbitals share their electrons between more than two atoms to form a delocalized $\pi$-bond. The $\pi$-bonds become delocalized along the chain and form a one-dimensional electronic system. The resulting 1D-band, has a considerable band width (on the scale of an eV), with a filled valence band originating from the HOMOs and an empty conduction band originating from the LUMOs, as shown in Figure 3. In Figure 4, molecular structure of other conjugated polymers is depicted.[9]

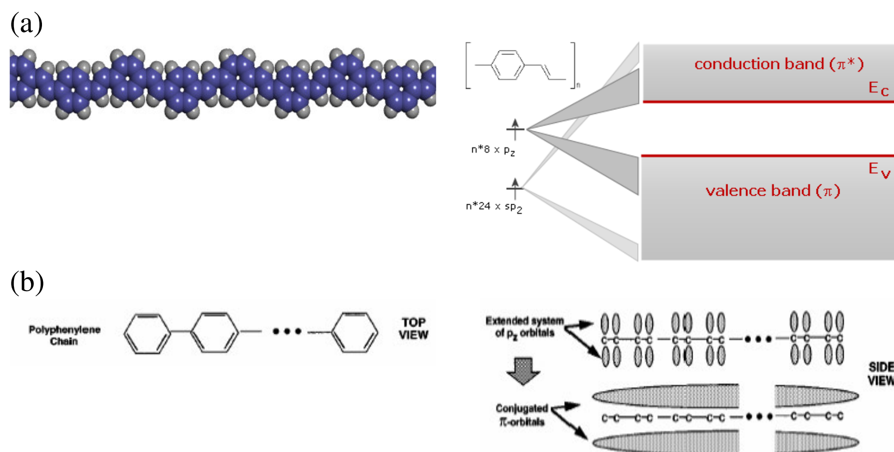


**Fig. 3** (a) Scheme of a polyphenylene and its energy levels (b) Schematic diagrams of the chemical structures and the molecular orbital structures for polyphenylene. [10]

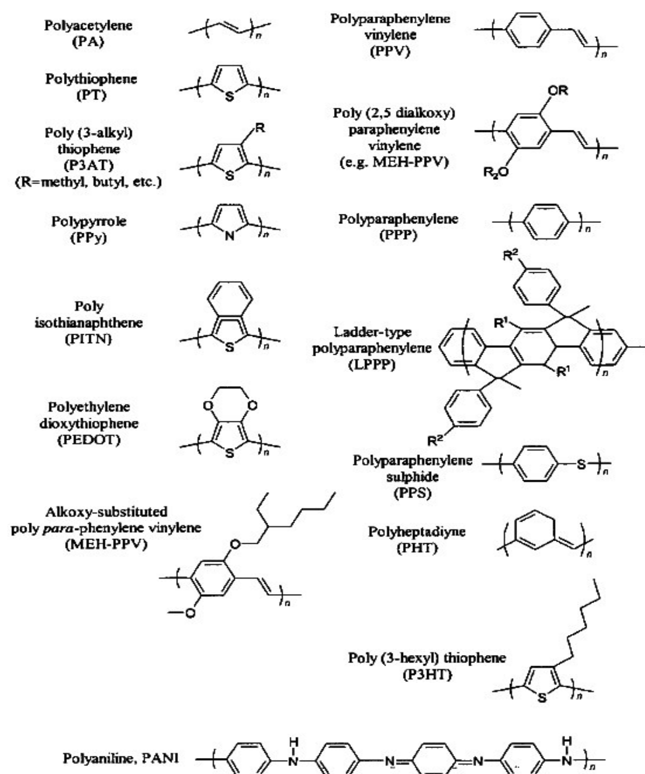


**Fig. 4** Molecular structure of various semiconducting polymer.[11]

## 1.2 Charge Transport in Organic Semiconductors

In metals and conventional semiconductors, charge transport occurs in delocalized states, and is limited by the scattering of carriers, mainly on phonons. Such a model can not be used in low conductivity materials such as amorphous or organic semiconductors. Although, the exact nature of charge transport in organic semiconductors is still not completely understood, it seems in these materials, transport occurs by hopping of charges between localized states. Because a simple estimate shows that the mean free path of carriers is lower than the mean atomic distance.[4] In conjugated polymers the polymer chains are weakly bound by van der Waals forces. They typically have narrow energy bands, HOMO and LUMO, which can easily be disrupted by disorder. Although electric charge is delocalized along the $\pi$-conjugated segments of the polymer backbone,

the length of such perfectly conjugated segments is typically limited to length scales of around 5 nm, separated by chemical defects, such as a non-conjugated $sp^3$-hybridized carbon atom on the polymer backbone, or by structural defects, such as chain kinks or twists out of coplanarity. Due to disorder, the semiconductor can not be regarded simply as having two delocalized energy bands separated by an energy gap. Instead, the charge transporting sites, which are the segments of the main chain polymer, are subject to a Gaussian distribution of energies, implying that all states are localized. Charge carriers move from one localized site to another localized site, on chain as well as between chains, Figure 5. It can be concluded that the charge transport and semiconducting properties of polymeric semiconductors are sensitive to the morphology of the polymer chains and the local structural order within the film.[12] The width of the Gaussian density of states is determined by the spatial and energetic disorder within the semiconductor and can be determined by temperature-dependent mobility measurements. A broad density of states leads to lower mobilities and a stronger temperature dependence.[13]

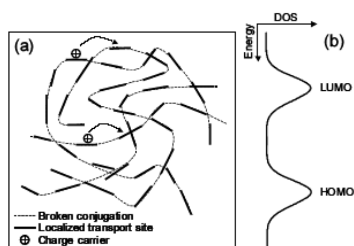


**Fig. 5** (a) Schematic view of polymer chains broken up in conjugated segments, which are represented as charge transport sites, between which the charge carries hop. (b) A representation of density of states which is often approximated by a Gaussian distribution for HOMO and LUMO levels.

### 1.2.1 Charge Carriers in Conjugated Polymers

Localization in conjugated organic materials occurs via the formation of polarons. A polaron is created by deformation of the conjugated chain. In other words, in a conjugated molecule, a charge is self-trapped by the deformation which it induced itself in the chain. This mechanism of self-tapping is often described through the creation of localized states in the gap between the valence and the conduction bands.[4]

### 1.2.2 Hopping Transport

Due to disorder and the localization of charge, the motion of carriers in organic semiconductors is typically described by hopping transport, Figure 6, as described before. This hopping transport takes place around the Fermi level. Depending on the structural and energetic disorder of the system, it can be energetically favorable to hop over a longer distance with a low activation energy (energy difference between sites), than over a shorter distance with a higher activation energy.

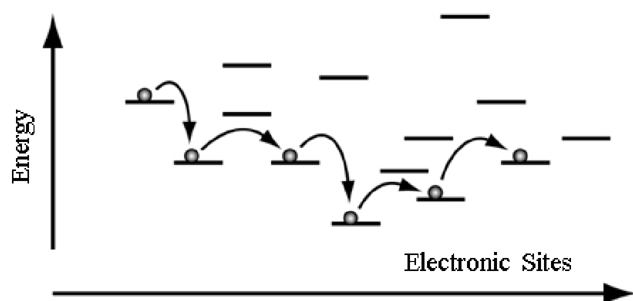


**Fig. 6** Hopping transport

### 1.2.3 Multiple Trapping and Release Model

For polycrystalline organic semiconductor layers the temperature dependent transport data is often interpreted in terms of a multiple trapping and release (MTR) model. In this model the organic semiconductor film consists of crystallites which are separated from each other by amorphous grain boundaries. In the crystallites the charge carriers can move in delocalized bands, whereas in the grain boundaries they become trapped in localized states.[11] In MTR model, a narrow delocalized band is associated with a high concentration of localized levels that act as traps. During their transit through the delocalized levels, the charge carriers interact with the localized levels through trapping and thermal release. The following assumptions are usually made: first, the carriers arriving at a trap are instantaneously trapped with a probability close to one. Second, the release of trapped carriers is controlled by a thermally activated process.[4]

## 1.3 Applications of Semiconducting Polymers in Molecular Electronic Devices

Owing to the unique electrical and optical properties of conjugated materials, several potential, technological and commercial applications such as diodes, LEDs, FETs, memory, photovoltaic cells, biosensing devices and display devices have been developed. In the following the basic principals for the operation of an OFET are given.

### 1.3.1 Organic Field Effect Transistors; The Basics

An organic field-effect transistor is composed of following components: a thin semiconducting layer, which is separated from gate electrode by the insulating gate dielectric; source and drain electrodes of width *W* (channel width) separated by a distance *L* (channel length) that are in contact with the semiconducting layer.

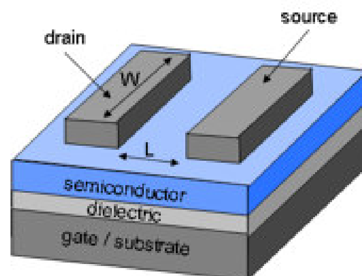


**Fig. 7** Geometry of an OFET

The gate can be a metal or a conducting polymer, but very often, is highly doped silicon which is used both as a substrate and as gate electrode. For gate dielectrics, inorganic insulators, such as $SiO_2$, $Al_2O_3$, and $Si_3N_4$, or polymeric insulators such as poly (methylmethacrylate) (PMMA) or poly(4-vinylphenol) (PVP) are commonly used depending on the transistor structure. The source and drain electrodes, which inject charges into the semiconductor, are usually high work function metals such as gold (also Pd, Pt, and Ag) or a conducting polymers (PEDOT: PSS, PANI) which can be printed.[13]

Voltage is usually applied to the gate electrode ($V_G$) and the drain electrode ($V_D$). The source electrode is normally grounded ($V_S$=0). The potential difference between the source and the gate is usually just called the

gate voltage, and the voltage applied between the source and drain is referred to as the source-drain voltage ($V_{DS}$). When there is no potential difference between source and drain like metal-insulator-semiconductor (MIS) for negative $V_G$, positive charges (holes) will be accumulated in the semiconductor. OFETs typically show p-type, but not n-type characteristics. The number of accumulated charges is proportional to $V_G$ and the capacitance $C_i$ of the insulator. In the equilibrium situation the Fermi levels of the gate metal and the semiconductor align due to the charge carriers, which move to or from semiconductor/insulator interface. When a voltage, called flat-band voltage, $V_{fb}$, equal to the difference between the Fermi levels of the materials is applied no band bending will be present in the semiconductor at the semiconductor/insulator interface, Figure 8(a). However, not all induced charges are mobile and will thus contribute to the current in a field-effect transistor. Deep traps first have to be filled before the additionally induced charges can be induced. That is, a gate voltage has to be applied that is higher than a threshold voltage $V_{Th}$ , and thus, the effective gate voltage is $V_G$-$V_{Th}$. In Figure 8(b) the positions of HOMO and LUMO of the organic semiconductor relative to the Fermi levels of the source and drain contacts for different applied gate and source-drain voltages are shown. If a negative bias is applied to the gate, the voltage drop across the insulator will accumulate holes at the semiconductor/insulator interface and the energy bands are bent upwards. The additional positive charges accumulated in this region are supplied by the Ohmic drain- and source contacts, because they are injecting electrodes. These charges are mobile and under a small drain bias will give rise to the filed-effect current. In Figure 8(c), the situation for applying positive gate voltage depicted which the bend is shifted downward approaching HOMO of the polymer. [13]

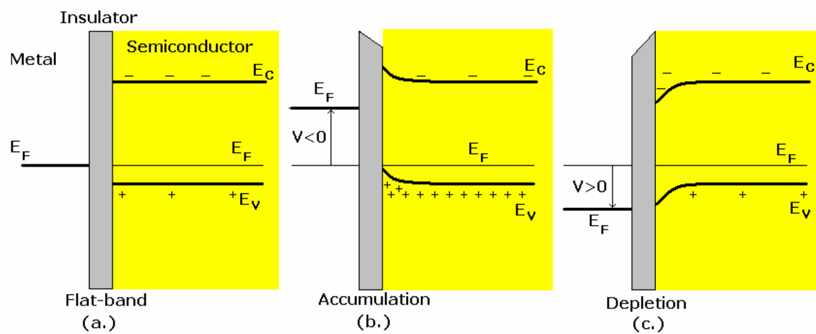


**Fig. 8** Energy-band diagram of a p-type MIS-FET working in: a) flat-band; b) accumulation; c) depletion region.

When no source-drain bias is applied, the charge carrier concentration in the transistor channel is uniform. When a small source-drain voltage is applied ($V_{DS}$<< $V_G$) the source-drain current increase linearly with the source-drain voltage, which is called the linear regime , in which the current flowing through the channel is directly proportional to $V_{DS}$. The potential $V(x)$ within the channel increases linearly from the source (x=0, V(x)=0) to $V_{DS}$ at the drain electrode (x=L,V(x)=$V_{DS}$). The output current is derived from the following formula

$$I_{DS} = \frac{W}{L} C_i \mu_{lin} (V_G - V_T) V_D \qquad (1)$$

Where W and L are the width and length of the channel respectively, $C_i$ is the capacitance of the insulator layer per unit area, and $V_T$ is the threshold voltage were the transistor turns on. When the source-drain voltage is further increased, a point $V_{DS}=V_G-V_{Th}$ is reached, at which the channel is “pinched off”. That means a depletion region forms next to the drain because the difference between the local potential V(x) and the gate voltage is now below the threshold voltage. A space-charge limited saturation current $I_{DS,Sat}$ can flow across this narrow depletion zone as carriers are swept from pinch-off point to the drain by the applied high electric field in the depletion region (Figure 9). Further increasing of the gate potential leads to an expansion of the depletion region and thus a slight shortening of the channel. Since the potential at the pinch-off point remains $V_G-V_{Th}$ and thus the potential drop between that point and the source electrode stays approximately the same $V_{DS} \sim V_G-V_{Th}$, the current saturates at a level $I_{DS,Sat}$ . The current in this case is given by the following formula

$$I_{DS} = \frac{W}{2L} C_i \mu_{sat} (V_G - V_T)^2 \qquad (2)$$

### 1.3.2 Mobility

As the number of transistors increases, the circuits should be characterized by low power dissipation and greater operation stability. The switching speed of organic integrated circuits can be estimated from the performance of the individual transistors and is roughly proportional to ~ $\mu_{FE}/L^2$, where L is the channel length of the transistor, and $\mu_{FE}$ is the field-effect mobility.[14] Thus efforts to find the material with higher mobility and make transistors geometry smaller are important.[15] Although several organic materials show

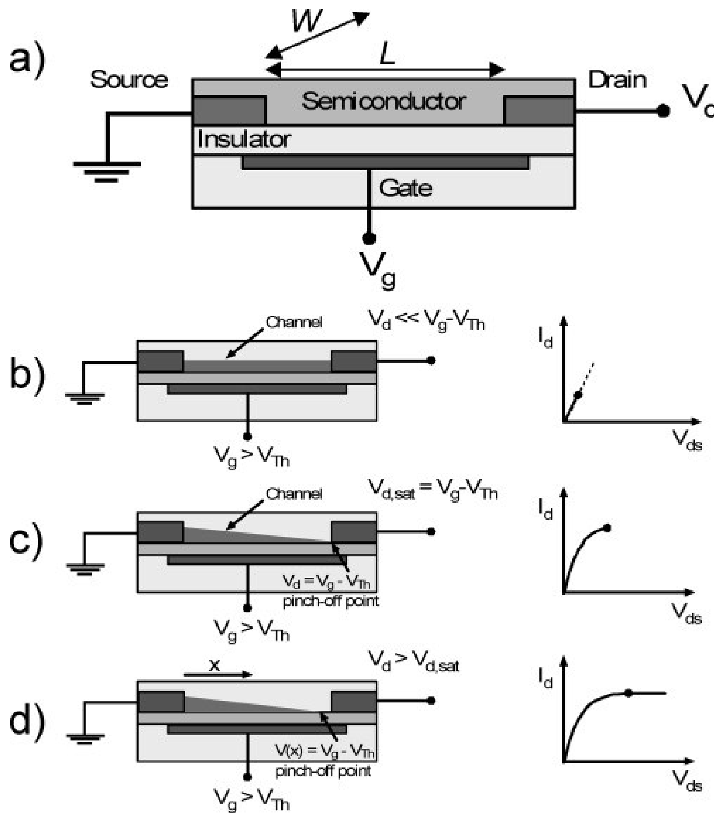


**Fig. 9** (a) Schematic structure of a field-effect transistor and applied voltages: L= channel length; W= channel width; $V_d$= drain voltage; $V_g$= gate voltage; $V_{Th}$= threshold voltage; $I_d$ = drain current. (b-d) Illustrations of operating regimes of field-effect transistors: (b) linear regime; (c) starts of saturation regime at pinch off; (d) saturation regime and corresponding current-voltage characteristics.[13]

high field-effect mobility, the mobility in the polymers in general compare to their inorganic counterparts relatively is low. Because charge transport along the chain is easy but between the chains is difficult. Conventional analysis (gradual channel approximation) for the calculation of the mobility in the OFETs is normally used. Gradual channel approximation states that the electric field along the channel is much lower than that across it. Because the thickness of the insulator is much lower than the source-drain distance, this statement remains valid even when the drain voltage compares to the gate bias.[16] This parameter is relatively easy to extract using standard equations. From linear formula, given above, one can derive the field-effect mobility of the polymer if geometry of the device and the capacitance of the

insulator are known once the device is measured. The mobility can be derived form the following formula:

$$\mu_{FE,linear} = \frac{L}{WC_i V_{DS}} \left. \frac{\partial I_{DS}}{\partial V_G} \right|_{V_{DS} \to 0} \qquad (3)$$

The mobility in the saturation regime can be calculated from analysis of current in this regime:

$$\mu_{Sat} = \frac{L}{2WC_i I_{D,Sat}} \left( \frac{\partial I_{D,Sat}}{\partial V_{GS}} \right)^2 \qquad (4)$$

Thus, mobility depends on the channel length (also on W and $C_i$) of the transistor, which means that the extracted mobility is a device parameter rather than a material parameter of the organic semiconductor. Ohmic contacts are assumed in deriving the equations above, meaning that the HOMO in the p-channel and LUMO in the n-channel transistors are aligned with the Fermi energy of the contacts in such a way that the injection barrier for the charge carriers is almost negligible. But what happens when there is a relatively big mismatch between the energy levels of the polymer and the Fermi energy of the electrodes? In this case there is a big resistance for the injection of charges into the polymer due to contacts and, consequently, a large contact resistance is anticipated. [17]

### 1.3.3 Contact Resistance and Injection

In all these devices, metal electrodes are utilized to inject charge into (or extract charge from) the organic semiconductor layer(s). The injection depends on parameters such as the energy barrier at the interface, the carrier mobility of the organic semiconductor, its carrier density (doping level), the presence of mobile ions, and the device geometry.[18] Despite its importance, the physics of charge injection in organic semiconductors remains poorly understood. This is somewhat surprising since contact resistances in organic transistors are within typically 10 kΩcm–10 MΩcm large compared to their inorganic counterparts. [11]

### 1.3.3.1 Scaling Behavior

As mentioned above, the mobility extracted from standard equations is a device parameter rather than a material parameter. To be able to evaluate the performance of the organic semiconductor, a correction for the contact resistance, $R_C = R_s + R_d$, is required. A theoretical approach to this end was presented by Horowitz.[19] In a transistor with the field-effect mobility $\mu$ and contact resistance $R_c$, the contact resistance to a good approximation is independent of the channel length $L$, but the actual channel resistance scales with $L$ and in linear regime is given by the $R_{ch}=L/W\mu en$ (where $n$ is the areal density of charge). Therefore, a critical channel length $L_c=\mu enR_c$ can be defined for which $WR_{ch}=R_c$ so that the contacts and the channel contributes equally to the total transistor resistance. Only transistors with a channel length clearly larger than $L_c$ can be expected to show "clean" TFT operation. Transistors with channel lengths such that $L \leq L_c$ become (severely) contact limited, meaning that the source–drain voltage mainly drops over the contact regions rather than over transistor channel and the overall transistor current is thus reduced.[20] The key feature of contact resistance is the nonlinear increase of the output characteristics at low drain voltages, highlighted in Figure 10. The presence of such non-Ohmic contact (or additional resistance) reduces the transistor current considerably in the low drain-bias regime.

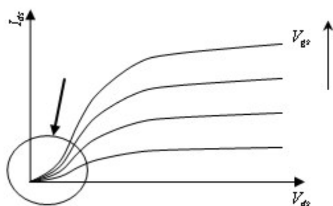

**Fig. 10** Output characteristic of a transistor and appearance of the contact effect.

### 1.3.3.2 Material Dependence

The contact resistance depends crucially on the materials used for the electrodes, meaning that it depends on the electrode work function as well as on the position of the HOMO level in case of a p-type polymer (or position of the LUMO level; in case of an n-type polymer). Moreover, there

is a clear correlation between the estimated Schottky barrier $\varphi_b$ and the contact resistance in such a way that the higher the $\varphi_b$ the higher is the contact resistance.[20]

#### 1.3.3.3 Sample Geometry

There are the three common geometries can be found for OFETs (in relation to the substrate): the bottom contact/bottom gate (BG/BG), bottom contact/top gate (BC/TG) and top contact/bottom gate (TC/BG) structures, as shown in Figure 11.

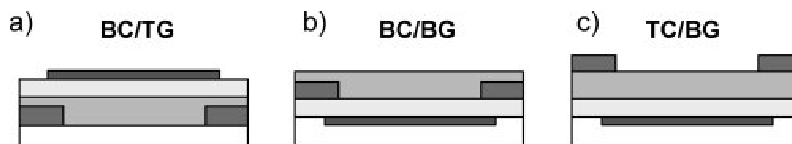


**Fig. 11** Common field-effect transistor configurations: (a) bottom contact, top gate (BC/TG); (b) bottom contact, bottom gate (BC/BG); (c) top contact, bottom gate (TC/BG).

The position of the injecting electrodes in relation to the gate is a major difference. In the BC/BG structure, charges are directly injected into the channel of accumulated charges at the semiconductor-dielectric interface. In the other two structures, the source/drain electrodes and the channel are separated by the semiconducting layer. Thus, charges first have to travel through several tens of nanometers of undoped semiconductor before they reach the channel. However, in the BC/TG and TC/BG configurations, charges are injected not only from the edge of the electrode but also from those parts of the electrode that overlap with the gate electrode, the top area of the electrodes. [13]

#### 1.3.3.4 Origin of Contact Resistance

There are two mechanisms that contribute to the contact resistance: charge carrier injection and bulk transport in the polymer before the charge carriers reach the accumulation layer at the insulator/polymer interface. The experimental fact reveals that for FETs with relatively small $\varphi_b$ (Schottky barrier), the contact resistance is dominated by the mobility of the polymer, and therefore the bulk transport in the polymer. On the other hand,

appreciable $\varphi_b$ indicates that the injection of charge carriers at the source contact (or drain) contributes predominantly to the contact resistance. To deal with this, one may use a simplified low-frequency equivalent polymer FET circuit where the conduction path between the source and drain is divided into a series of three resistive elements:

$$R_{s\text{-}d} = R_s + R_{ch} + R_d = R_C + R_{ch} \qquad (5)$$

where $R_{s\text{-}d}$ is the transistor resistance, $R_s$, $R_{ch}$, $R_d$, are the source, channel and drain resistance respectively and $R_C$ is the contact resistance. So the overall contact resistance $R_c = R_s + R_d$ is sum of two parts where $R_s$ originates from the injection of charge carriers and transport through a narrow region in front of the source contact where no accumulation layer forms, and also the bulk resistance. $R_{ch}$ is the gate-modulated channel resistance and $R_d$ is the resistance arising from the extraction of charge carriers at the forward biased drain contact.[21]

The energy level diagram of holes in an ideal bottom contact FET is shown in Figure 12 where the lateral extents of the accumulation layer ($a$) and the depletion zone at the contacts ($d$) are largely exaggerated for clarity. The strong band bending associated with the formation of the depletion zone ($d$) is only possible in the high gate potential model, and is due to the absence rather than presence of net space-charge in this region, a peculiarity of the two-dimensional electrostatic problem with a gate electrode close by. The bands are flat in the virtually undoped bulk of the polymer. Due to electric-field-induced barrier lowering the main paths of current flow at the contacts are within a few nanometers of the polymer/insulator interface, as indicated by arrows.

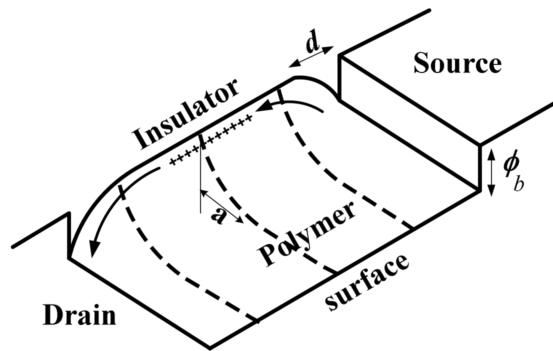


**Fig.12** Energy level diagram for holes in an ideal bottom contact FET.

### 1.3.4 Transfer Line Method

The question is still remaining: what happens with the mobility when the contacts are not Ohmic? Mobility is an intrinsic property of the material and it should be independent of the contact. The gradual channel approximation can not be valid for an OFET with a nonlinearity in the linear part of its output characteristic, where the contact resistance is more pronounced. Another method is the transfer line method (TLM) which is used to separately determine the contact resistance and the mobility. This method which has been applied previously to α-Si:H transistors, is based on the fact that the channel resistance is proportional to the channel length, while the contact resistance is independent of it. The method consists of measuring the drain current under similar gate and drain voltages on devices with various channel lengths.

The transfer line method test structure consists of depositing a metal grid pattern of unequal spacing $L_i$ between the contacts. This leads to a scaled planar resistor structure.[22] Each resistor changes only by its distance $L_i$ between two adjacent contacts, as shown in Figure 13 and it can be expressed by

$$R_i = \frac{\rho_s L_i}{W} + 2R_C \qquad (6)$$

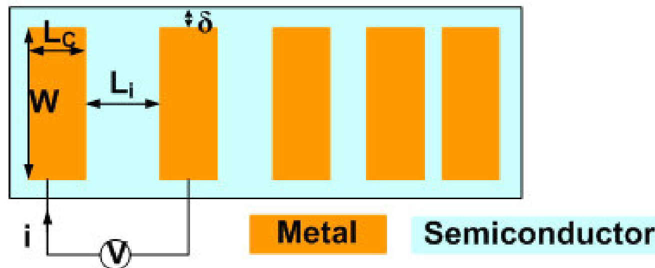


**Fig. 13** transfer line method test structure.

Then, by plotting the measured resistances as a function of the contact spacing $L_i$, according to Equation 6, the layer sheet receptivity $\rho_s$ and the contact resistance $R_c$, can be deduced from the slope and from the intercept at $L_i$=0 respectively, as shown in Figure 14. The main advantage of the TLM method is its ability to give two main electrical parameters, the resistivity of the semiconductor $\rho_s$ and the contact resistance $R_c$.

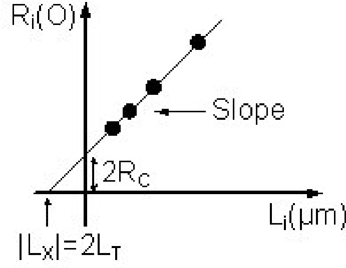


**Fig. 14** The plot of the $R_i$ versus $L_i$. Slope= $\rho_s$/ W, $R_i$ (intercept)=2$R_c$; and |$L_i$ (intercept)| =2$L_T$

In practice, we plot the total device-resistance, $R_{ON} = V_{ds}/I_{ds}$, as a function of the channel length, $L$, for different gate voltages ($R_{ON}$ by definition is the same as $R_i$ in the above discussion). In the linear operating regime of the transistor the channel resistance varies linearly with the channel length. The contact resistance, $R_C = R_s + R_d$, at the source and drain contacts is assumed to be independent of $L$. The $R_{ON}$ can then be expressed as:

$$R_{ON} = \left.\frac{V_{ds}}{I_{ds}}\right|_{V_{ds}\to 0} = R_{ch}(L) + R_C \tag{7}$$

The experimental data are, in first order, well described by this equation, with $R_{ON}$ depending linearly on $L$. From the slopes of the plots we find the channel resistance, $R_{ch}$, the inverse of which, $[\Delta R_{ON}/\Delta L]^{-1}$, is the channel conductivity. From the derivative of the channel conductivity, the field-effect mobility, corrected for $R_C$ can be obtained:

$$\frac{\partial([\frac{\Delta R_{ON}}{\Delta L}]^{-1})}{\partial V_g} = \mu_{FE}(V_g)WC_i \tag{8}$$

The resulting corrected mobilities yields a higher overall $\mu_{FE}(Vg)$. From the analysis with this method one can find $R_C$ as the intercept of $R_{ON}$ at $L = 0$. This intercept depends on the applied gate voltage, which implies that $R_C$ decreases with increasing gate voltage, so clearly the contact resistance is strongly gate bias dependent. There is a general agreement that the decrease of the contact resistance is correlated to the higher density of charge in the conducting channel at high gate voltages.

### 1.3.5 Interface

OFETs are interface devices, typically operating in accumulation mode and only the first two molecular layers next to the dielectric determine the charge transport.[15] Therefore, detailed investigations of the growth of the morphology as well as molecular orientation close to the molecule/substrate interface are of great interest. Charge carrier transport in the OFETs operation is strongly dependent on the properties of the two involved interfaces: interface between semiconductors and electrodes, where charge injection occurs from the electrodes into the semiconductors and interfaces between semiconductors and insulators, where charge transport takes place in the semiconductor layer. The properties of these interfaces determine the device performance, thus a great deal of research has focused on interface engineering.[23] The interface between semiconductor and insulator is important in the OFET device, because the charge transport occurs in the first two molecular layers next to the dielectric interface. In the bottom gate configuration trapping of charges at the semiconductor-dielectric interface is done by hydroxyl groups, present in the form of silanols in the case of commonly used $SiO_2$ dielectric.[24] Normally, organic dielectrics are used in top gate OFETs in which the interface can exhibit a large number of chemical groups that can act as charge-carrier traps; this will have a detrimental influence on charge-carrier transport within the channel. The modification of the interface, on the other hand, can be used to increase and facilitate the charge transport.[15]

Thus engineering the interface of the semiconductor/ insulator and/or semiconductor/ electrodes by using surface dipoles, physical treatment, and self-assembled monolayer (SAMs) is receiving significant attention as the latest approach for enhancing the electrical properties of organic semiconductors.[23]

## 1.4 Self-Assembly in the electronic devices

Recent advances in molecular electronics have created a large interest in metal/organic interfaces. Transport of charge carriers across the interfaces between metal electrodes and the organic material often determines the performance of a device. Thus manipulation of the injection barrier at the metal/polymer interface is of interest. Changing the injection barrier will result in either facilitating charge injection and therefore

improving the performance of the device or reducing the charge injection and degrading the performance.[25] Engineering of the injection barrier is achieved through manipulating of either the HOMO (or the LUMO) of the polymer, or by modifying the work function of the electrodes. Self-assemblly of monolayers is a technique which can insert polar molecules onto metals and modify the metal-(semi-conducting) polymer interface.

It has been shown that self-assembled monolayers (SAMs) can change the work function of the metals; however this effect was not clear in the electronic devices.[8] Recently de Boer et al. modified the Au-coated (20 nm) glass substrates with SAMs of 1H,1H,2H,2H-perfluorodecanethiol (PFDT) and hexadecanethiol (HDT). They found for the untreated gold, the work function is 4.9 eV, whereas the SAMs of PFDT and HDT shift work function to 5.5 eV and 4.1 eV, respectively. In addition of improving charge injection, SAM-modified electrodes are also very useful in selectively blocking one type of charge carrier in optoelectronic devices. Also PFDT SAMs increase the work function of Ag ($\Phi_{Ag}$ ~ 4.4 eV) to 5.5 eV ($\Delta\Phi$~ 1.1 eV) and SAMs of HDT lowered $\Phi_{Ag}$ to 3.8 eV, and blocked hole injection into PPV, which enabled studying the electron transport in these devices (Figure 15). This method, demonstrates a simple and attractive approach to modify and improve metal/organic contacts in organic electronic devices like LEDs, PV cells, and FETs.
So the main idea in this project is using monolayer of molecules with inherent dipoles to tune the work function of the metal electrodes in the OFETs.

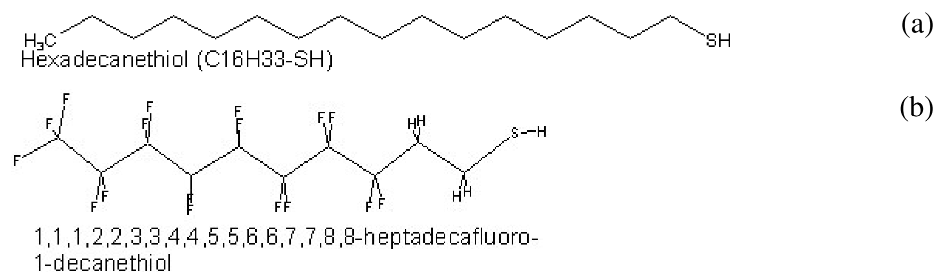


**Fig. 15** Two alkanethiols SAM molecules with opposing dipole moments namely (a) HDT: Length = 23.7 **Å**, Dipole = 1.955 D, (b) PFDT: Length =16.2 **Å**, Dipole = –2.276 D.

### 1.4.1 The Self-Assembly Technique

Atoms and molecules that are chemisorbed (or physisorbed) on the surface of metals can give an increase or decrease of the work function. Self-assembled monolayers (SAMs) systems are extensively used to study the effect of chemisorbed organic molecules on the metal work functions.[26] The self-assembly (SA) technique can be used to prepare monolayer or multilayers thin film. Each layer in a self-assembled film can be covalently linked and no excessive deposition can take place as the reactive sites on the layer surface is self-limiting. The SAM preparation step is shown in Figure 16. By dipping the solid substrate into the SAM solution, molecules are transferred to the substrate and, subsequently, highly ordered, two dimensional structures and densely packed molecular layer forms spontaneously on the substrate. Formation of the SAM is based on the strong interaction between the substrate and a surface-specific functional group of the adsorbent, for instance the sulphur compounds and a gold substrate. SAMs are good systems for surface modification, by changing in rigidity, length, and terminal functional group of the molecule, which in turn affects the uniformity, packing, conformation, polarity, and charge density of the surface. SAMs have been thoroughly characterized using a large number of surface analytical tools. Among the most frequently used techniques are infrared spectroscopy, ellipsometry, studies of wetting by different liquids, X-ray photoelectron spectroscopy, electrochemistry, and scanning probe measurements.[11]

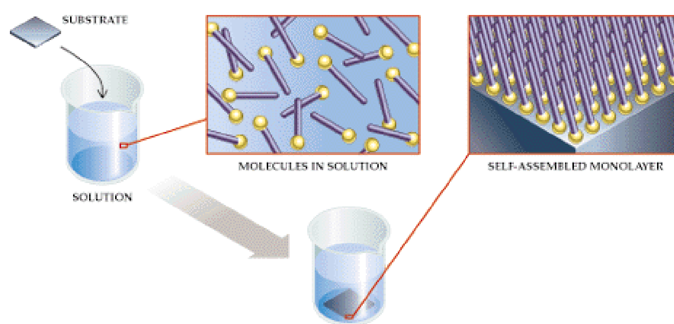


**Fig. 16** Self-Assembly Process

This self-assembly is specifically used for alkanethiols ($C_nH_{n+1}SH$) SAMs on the gold (111) or silver (111) surfaces and alkanethiols are well

known to self-assemble in a uniform and densely packed monolayer on metal surfaces.[4] The sulfur head of the molecules form stable covalent bonds to the gold or silver surface and their alkyl tails are close packed, which make a well-ordered monolayer. The thiols are believed to attach primarily to the threefold hollow sites of the gold surface, losing the proton in the process and forming a (√3×√3) R30° over layer structure, Figure 17, and the nearest neighboring distance in this geometry is 4.97 Å, resulting in an available area around 25 Å$^2$ for each molecule. Since the van der Waals diameter of the alkane chain is somewhat too small (4.6 Å) for the chain to completely occupy that area, the chains will tilt, forming an angle of approximately 30° with the surface normal.

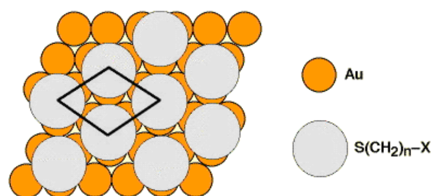


**Fig. 17** Schematic model of the (√3×√3)R30° overlayer structure formed by alkanethiolate SAMs on Au(111).

The bond strength of Au-thiolate is 44 kcal/mol and contributes to the stability of the SAMs together with the van der Waals forces between adjacent methylene groups, which amount to 1.4–1.8 kcal/mol. The latter forces add up to significant strength for alkyl chains of 10–20 methylenes and play an important role in aligning the alkyl chains parallel to each other in a nearly all-trans configuration. The difference between SAMs on the gold and silver is just the tilt angle of the molecule which in case of silver is around 12° instead of 30° for gold, which is due to the larger nearest neighbor spacing in the (111) plane for Ag ( lattice constant of Ag is 2.89 Å and on Au is 2.88)

Alkanethiol molecules adsorb from the dilute solution at room temperature and form packed monolayers in less than one hour. In solution, the adsorption time seems to be independent of the chain length, but the concentration has a crucial role as higher concentrations lead to shorter adsorption time. If the number of the carbon atoms is more than five, the process of ordering is slowed by strong chain-chain interactions. In all case, the adsorption stops at the monolayer level.

### 1.4.2 Work Function Change Induced by the Adsorbates

The work function, $e\Phi$, is defined as the energy difference between the Fermi level $E_F$ and the vacuum energy $E_{vac}$ and therefore it can be expressed as follows $e\Phi = E_{vac} - E_F$

The macroscopic interpretation of the work function contains several contributions. On the metal surface the major contribution is due to the fact that the electron density leaks out from the framework of the positive ion cores. This gives rise to a dipole layer at the surface, which the emitted electron must pass through. Adsorbed atoms and molecules generally have a significant influence on the electronic structure of the host surface. They rearrange the electronic charge within the chemical bond and may also add elementary dipole if the adsorbed molecule has its own static dipole moment and therefore it changes the work function of the surface. In the case of chemisorptions, charge is shifted from the adsorbed molecule, or vice versa, thus giving raise to additional dipole whose field acts on emitted electrons. This effect is described by a change of work function, $e\Delta\Phi$, due to adsorption.[11]

### 1.4.3 Tuning the Work Function by SAMs

The self-assembled monolayer can be seen simply as inserting a sheet of electric dipoles at the interface which in turn results in charge redistribution on the metal surface.

(a) (b)

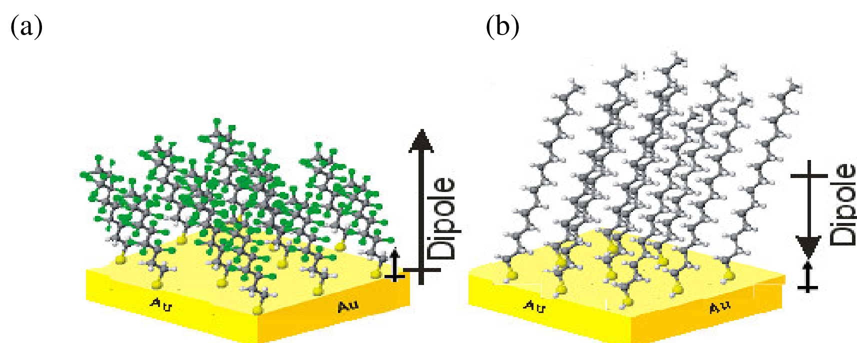


**Fig. 18** Electrical dipole moments of (a) 1*H*,1*H*,2*H*,2*H*-perfluorodecanethiol and (b) hexadecanethiol SAMs on Au(111) and Ag(111), there are two contributions; the small arrow is due to Sulphur-Metal dipole and the bigger arrow is due to polar end group of the SAM itself.

Hence there are two contributions in charge distribution on electrode's surface which determine the new work function of the electrode. One is the charge distribution on metal surface, the work function of metal itself, and the other is the electronic charge distribution on the surface introduced by monolayer, the dipole moment of the monolayer. From classical electrostatics one can calculate the potential drop caused by this dipole sheet, the change in work function can be written as:

$$\Delta\Phi = \int_0^l \frac{\sigma}{\kappa\varepsilon_0} dx = \frac{\sigma l}{\kappa\varepsilon_0} = \frac{Nql}{\kappa\varepsilon_0} = -\frac{N\mu_{\perp,SAM}}{\kappa\varepsilon_0} \quad (9)$$

where $\sigma$ is the surface charge distribution, $l$ is the thickness of the layer, $\kappa$ is the dielectric constant, $\varepsilon_0$ is the permittivity of vacuum, $N$ is the grafting density of self assembled molecules and $\mu_{\perp,SAM}$ is perpendicular component of dipole moment of the layer. To calculate the shift, one has also to take into account the dipole moment of the S–Au layer. By doing so, the formula becomes:

$$\Delta\Phi = -N\left[\frac{\mu_{\perp,SAM}}{\varepsilon_0 k_{SAM}} + \frac{\mu_{M-S}}{\varepsilon_0 k_{M-S}}\right] \quad (10)$$

The effective Sulphur-metal dipole is assumed to be almost independent of the alkane chain length and composition, but strongly dependent on the nature of the metal. For alkanethiol SAMs, the effective S-metal dipole has an opposite, but smaller value than the effective dipole of the SAM itself, which result in a smaller shift of the work function when compared to the perfluorinated alkanethiols. In that case an effective S-metal dipole is in the same direction as that of the monolayer (Figure 18).

Tuning the work function of the metallic electrode by the SAM has an important effect on the carrier injection, especially when these layers are used as an interlayer between electrodes and semiconducting polymers. This effect is illustrated in Figure 19, where by using HDT SAMs the position of the work function of metal is changed compare to the HOMO of the polymer. The injection barrier for holes is increased. Using the opposite dipole moment of the PFDT SAM, Ohmic contacts for hole injection between electrode and semiconducting polymer can be created.

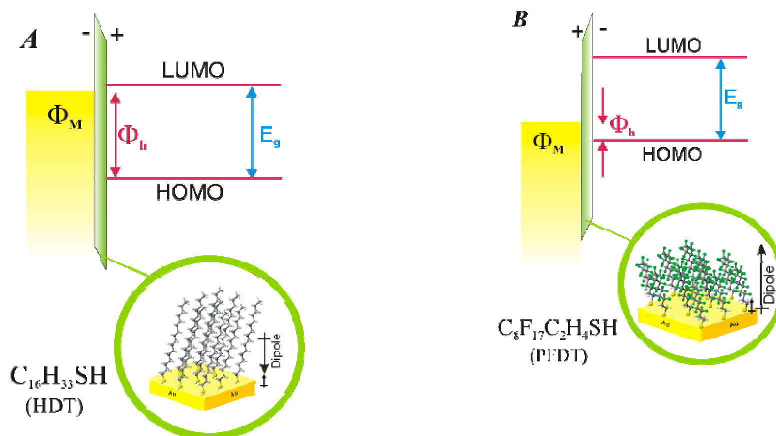


**Fig. 19** Schematic energy diagram of metal/SAM/organic interface; (A) lowering the work function of electrode, (B) raising the work function of electrode.

Other alkanethiols with different length are also used as SAMs in our experiment in the OFETs (Figure 20). The work function shows only little variation for alkylthiolates with different chain lengths because both $\mu_{SAM}$ and $\mu_{S\text{-}M}$ only weakly depend on the length of the alkyl tail.[26] The dipole $\mu_{S\text{-}M}$ resulting from chemisorption of the alkylthiols is mainly determined by the metal-sulfur bond. Both the dipole moment of an alkylthiols molecule and the orientation of the molecule in the SAM do not vary strongly with the length of the alkyl tail. Therefore, $\mu_{SAM}$ weakly depends on the length of the alkyl group. [26]

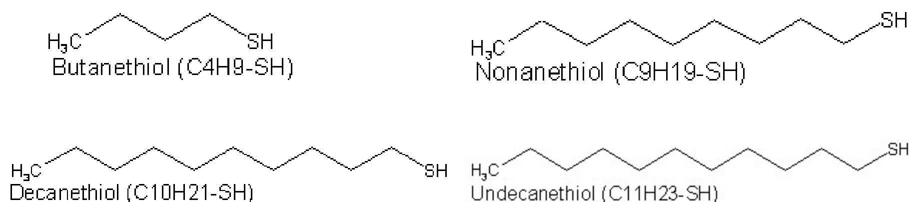


**Fig. 20** Different alkanethiols used in our experiments; butanethiol: Length = 8.5 Å, nonanethiol: Length = 14.8 Å, decanethiol: Length = 16.0 Å, and undecanethiol (UDT): Length = 17.3 Å.

### 1.4.4 Charge transport in Self-Assembled Monolayer

Charge transport through individual molecule is different from the bulk transport because of the inherently small size of molecule. Alkanethiols

SAM are not conjugate molecules, thus they are like a very thin insulator layer between the metal and semiconductor. However, they have a very low resistance compare to the polymer and, consequently, can be neglected. The transport is done by tunneling of the charges thorough this small barrier.[27]

The Figure 21, shows when one takes the data from single molecule measurements and extrapolates this to contact area of SAM in organic devices, we can regard this as a large number of parallel resistor, which do not contribute to the total resistance due to its large Number. Also by increasing the length of the molecules the resistance increases exponentially.

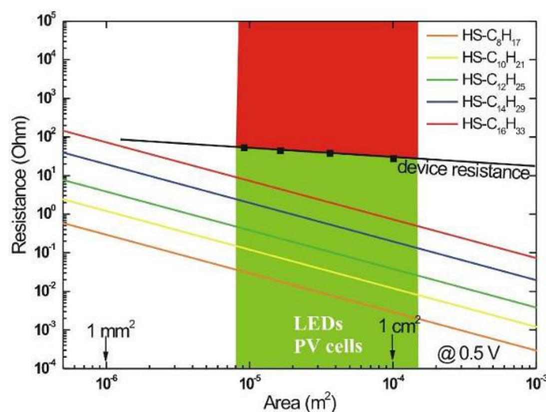


**Fig. 21** Resistance of alkanethiols SAMs versus area.

### 1.4.5 Applications of the SAMs on gate insulator

Besides using the SAMs for tuning the charge injection in electronic devices, it has been demonstrated that the interfacial layers formed by SAM of hexamethyldisilazene (HMDS) or octadecyltrichlorosilane (OTS) on silicon oxide at insulator-semiconductor interface of an OFET, improves the wetting of the polymer, especially rr-P3HT. This avoids disordered films, poor performance and the mobility of the charge carriers is increased due to morphological changes.[25] Because charges in the polymer are trapped at polymer and bare SiO2 interface due to hydroxyl groups or other interface states. Electrical measurements lead to lower current output which results in lower values of the mobility for polymer semiconductors.

# Chapter 2

# Experiments (Part 1)

The project is basically divided into two parts. In the first part of the experiments, the effect of the self-assembled monolayer (SAM) was shown on the gold electrodes in the field-effect transistors using MEH-PPV, rr-P3HT and PFO as the semiconducting polymer. The transistors were BC/BG configuration, fabricated by lithography and delivered by Philips. In the second part, after the processing of the dual gate configuration OFETs, the effect of the SAM on the gold and silver electrodes in the BC/BG and BC/TG was investigated.

Our standard FET test substrates were prepared by Philips, Eindhoven. These field-effect transistors were made using heavily doped silicon wafers as gate electrode with a 200 nm thick layer of thermally oxidized $SiO_2$ as gate dielectric. By conventional photolithography, gold drain and source electrodes were patterned on top of the $SiO_2$. A 10 nm thick layer of titanium was used as adhesion layer for the gold on silicon oxide. In our experiments, the device was then treated with the primer HMDS in order to make the surface hydrophobic and to obtain a better defined interface between the gate dielectric and the semiconducting polymer. The device was finished by spin-coating the organic layer from solution. (Figure 22) The layer thickness was typically 200 nm. The solvents used were toluene and chloroform. In order to avoid contamination with water and oxygen, most of the polymers were spin-coated in the glove-box and then transported directly to the measurement set-up.

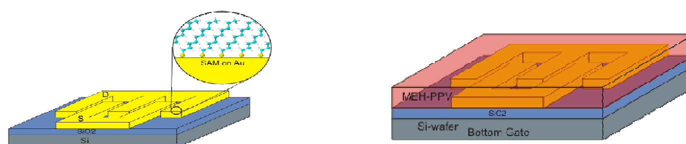


**Fig. 22** Schematic picture of using a SAM in the BC/BG OFET with a spin coated semicondcing polymer on top.

### 2.1 SAM preparation

Field-effect transistors are cleaned with ethanol and 2-propanol and then immersed in the ~1-3×$10^{-3}$ M solution of HDT or PFDT in ethanol (or other SAM solution) for different times, varying from 1 night to several days. Before depositing the semiconductor layer, samples were taken out of the solution, rinsed with ethanol, toluene and 2-propanol, respectively, and dried with a deionized $N_2$ flow. Next, the SAM-modified FETs were transferred to the glove box with $H_2O$ and $O_2$ concentration less than 0.1 ppm for spin coating the polymer.

### 2.2 Spin-Coating

The spin coating technique is used to apply uniform thin films to the flat substrates. An excess amount of the solution is placed on the substrate, and then the substrate is rotated at high speed to spread the fluid by centrifugal force. Rotation is continued while the fluid spins off the edges of the substrate. The solvents are volatile, and simultaneously evaporate, so the higher the speed of spinning the thinner the film due to the layer centrifugal force. The thickness of the film also depends on the concentration of the solution and the solvent.

Firstly, 3 mg of MEH-PPV was dissolved in 3 ml toluene and heated to 70°C over night. The spin coating program used for the SAM-modified FET and unmodified substrate is listed below. The resulting layer thickness was typically 200 nm.

| | Speed (rpm) | Acceleration (rpm/s) | Time (second) |
|---|---|---|---|
| 1- Open | 400 | 300 | 5 |
| 2- Close | 600 | 500 | 60 |
| 3- Open | 800 | 500 | 30 |

Furthermore, 3 mg of rr-P3HT was dissolved over night at room temperature in 3 ml chloroform and spin-coated with same program on the BC/BG transistors. Finally, the PFO solution is processed with a concentration of 30 mg/ml in toluene and was dissolved at room temperature over night and heated to 70°C one hour before spin coating on the FET substrates. Spin coating the PFO polymer on the FET device with the PFDT SAM is challenging because of the hydrophobicity of the surface. The spin coating program is given below.

| | Speed (rpm) | Acceleration (rpm/s) | Time (second) |
|---|---|---|---|
| 1- Open | 200 | 1000 | 5 |
| 2- Close | 1000 | 100 | 5 |
| 3- Open | 250 | 500 | 60 |

## 2.3 Electrical measurements

Electrical measurements were carried out in a home-built probe station under high vacuum ($10^{-6}$ mbar) with Keithley 4200 semiconductor analyzer at room temperature. Contact to the bottom gate is made by scratching off the siliconoxide layer, and to improve the contact, silver paste is applied. To prevent parasitic currents and to electronically isolate the gate potential a sheet of mica was used between the silicon gate of the devices and the copper chuck.

## 2.4 Results and Discussion (Part 1)

### 2.4.1 MEH-PPV

Poly(2-methoxy-5-(2'-ethylhexyloxy)-1,4-phenylenevinylene)(MEH-PPV) is an amorphous semiconductor with its HOMO at 5.2 eV (Figure 23).

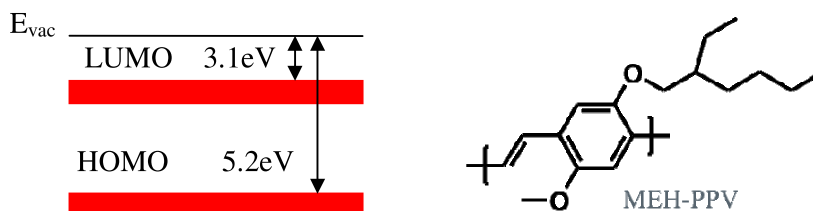


**Fig. 23** Schematic energy diagram of MEH-PPV and the chemical structure of the polymer.

Therefore a negligibly small injection barrier with gold is obtained, since the work function of vapor-deposited Au is ~ 4.9 eV (as measured with the Kelvin probe). The MEH-PPV/Au contact can be considered an Ohmic contact. Modifying the contacts with the HDT, results in a work function of ~4.0 eV and creates a large injection barrier of ~1 eV for the injection of holes. On the other hand, PFDT increases the work function of gold to 5.5 eV. In the latter case an Ohmic contact is expected.25

Output characteristics of the two sets of finger transistors with W/L=10000/20 are shown in Figure 24 and demonstrate the effect of different SAMs on the charge injection. The results show that HDT suppresses the current (both in linear and saturation regimes) of the transistors while in the case of PFDT, the output characteristics are almost unaffected compared to the untreated transistor.

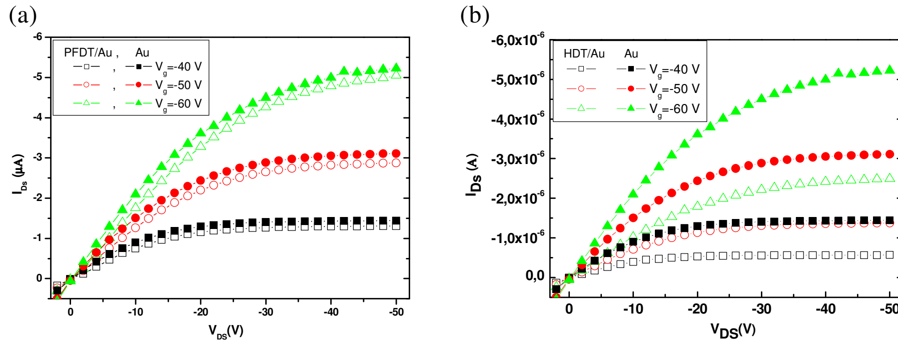


**Fig. 24** Output characteristics of a FET based on MEH-PPV with (a) untreated Au electrodes and PFDT-modified Au electrodes and (b) untreated Au electrodes and HDT-modified electrodes.

As expected, PFDT-modified Au contact with work function of 5.5 eV forms an Ohmic contact with MEH-PPV similar to untreated Au contacts. The small difference in the current between the PFDT treated and untreated transistor can be explained by the molecular monolayer at the metal/semiconductor interface, which can be regarded as a tunnel barrier at the interface that introduces an additional resistance at this interface. The FET characteristics of MEH-PPV with the HDT-modified Au electrodes demonstrate clearly that the large hole injection barrier suppresses the charge injection in these FETs. By investigating the transfer characteristics in the saturation regime, we derive the threshold voltage from the intercept of the linear fit to data. From the slope, the mobility can be extracted. As expected, both the untreated Au and Au modified with PFDT create an Ohmic contact, and, consequently, the slopes of the linear fits are similar, which implies similar apparent mobilities.

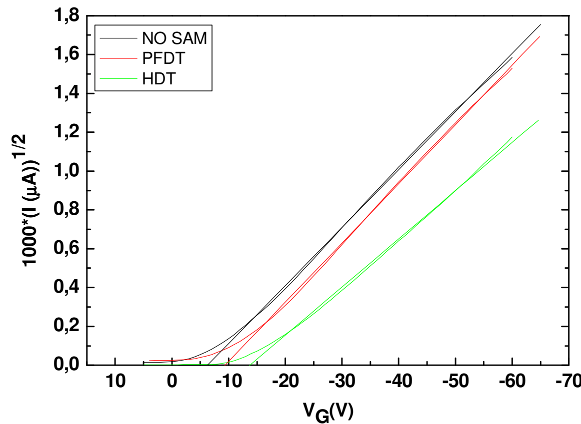


**Fig. 25** The transfer characterisitcs in the saturation regime and the increase of the threshold voltage for SAM-modified Au electrods in MEH-PPV-based transistors.

From this analysis the SAM apparently affects the mobility of charge carriers in MEH-PPV. Since MEH-PPV is an amorphous material, its charge transport is isotropic and governed by the concentration of charge carriers. Furthermore, as discussed before, the mobility is an intrinsic property of the material and independent of the geometry, morphology and contacts. A series of finger transistors with channel lengths of 7.5, 10, 15, 20, 30 and 40µm and channel width of 10000 µm were measured and the TLM method was applied. These measurements were repeated for FETs with their Au contacts modified with HDT and PFDT. The analysis resulted in the same mobility for both SAM-modified and untreated FETs of 4×10-3 cm 2V -1S -1 for MEH-PPV at low VDS (VDS= –2 V) and high VG. Figure 26 shows the calculated mobility and contact resistance of the transistors versus VG.

Furthermore, the analysis for the contact resistances of the HDT-, PFDT-modified and untreated FET demonstrates an increasing contact resistance with the length of the SAM. HDT raises the contact resistance in the low gate voltage regime by more than two orders of magnitude compared to the untreated Au contacts. PFDT on the other hand increases the contact resistance by less than one order of magnitude. In general, the contact resistances decrease when gate voltage is increased due to the increase of the induced charges and thus reduction of the injection barrier.
In conclusion, the contact resistance is modified when a SAM is applied while mobility remains the same by taking the appropriate analysis into account.

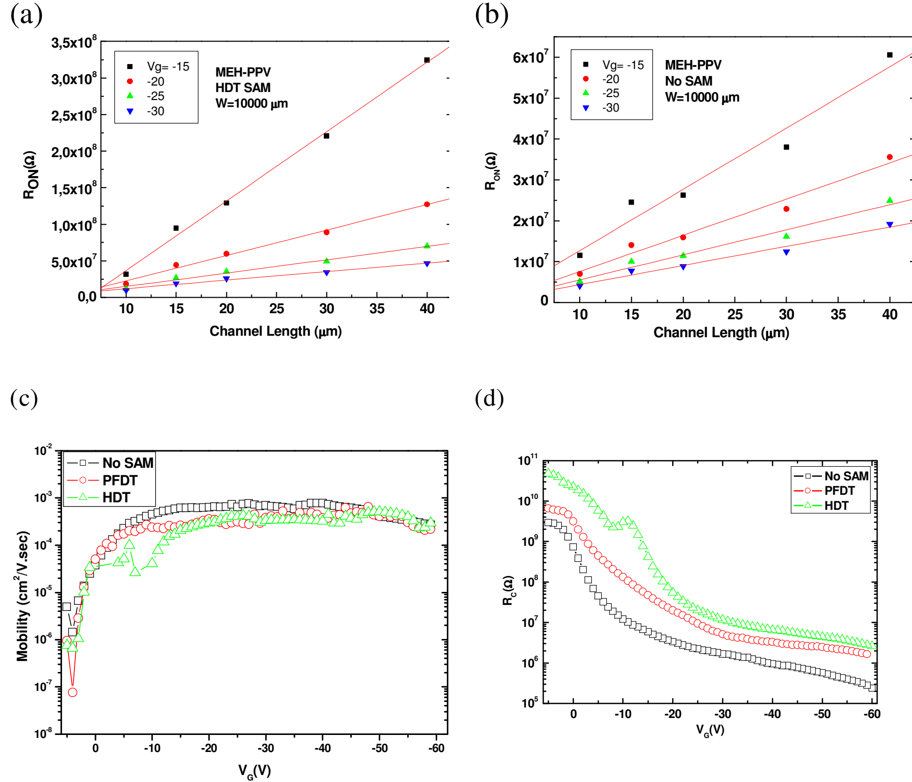


**Fig. 26** TLM analysis of the MEH-PPV based transistors at $V_{DS}$= -2 V: (a), (b) $R_{ON}$ versus channel length for unmodified and HDT-modified transistors. (c) Mobility and (d) Contact resistance of the unmodified, PFDT- and HDT-modified Au electrodes in OFETs.

As mentioned before, the contact resistance can be derived from the intercept of the liner fit to the data points at L=0 (Figure 14). Therefore calculation of contact resistance depends on the number of the measured transistors with different channel lengths. More data points results in a more precise calculation of the contact resistance. Consequently, suach a calculation can result in a negative contact resistance, which is physically meaningless. This is the main draw back of TLM method.

The mobility calculated from TLM is less sensitive because it is derived from the slope of the linear fit to the $V_{DS}/I_{DS}$ values, thus the variation of this slope leads just to mobilities of the same order of magnitude.

### 2.4.1.1 Threshold voltage

Another important parameter is the threshold voltage $V_T$ from both a technological and theoretical point of view. The threshold voltage can be defined as the gate voltage at which the conducting channel starts to form.
The OFETs operate in the accumulation regime so in principle, the threshold voltage should be zero. However, lots of charge carriers are trapped at the interface between the semiconductor and insulator. Traps induce a gate voltage dependent mobility, which results in the emergence of an on-set voltage. Below the onset, the mobility is very low and the current remains lower than the parasitic current. The current sets in when sufficient amount of traps are filled, which takes place through the gate potential which induce charge carriers and fills up the Fermi level at the insulator-semiconductor interface. Because this increase of the Fermi level corresponds to a very small fraction of the gate voltage, this contribution may lead to threshold voltage shifts of up to tens of volts.[16]

The threshold voltage can depend on the time a gate voltage has been applied (bias stress), on the exposure of the device to light or it can be shifted using a polarizable gate insulator. Furthermore, a dependence on the work function of the gate electrode and the thickness of the active layer material has been reported.[28] As we will see in Figure 27, threshold voltage depends on the work function of the electrodes. The average threshold voltage for HDT-modified transistor is higher than for PFDT or unmodified transistors.

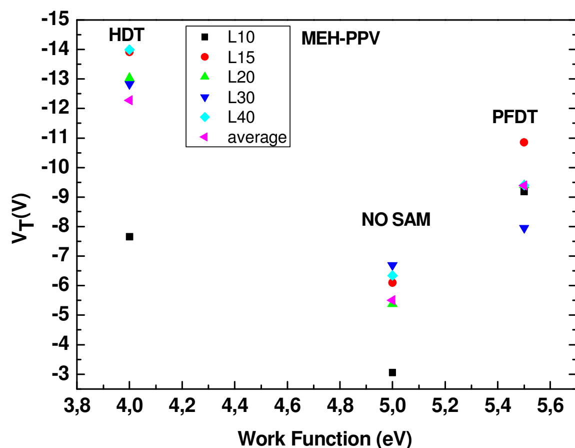


**Fig. 27** Threshold voltages versus work function of the electrodes.

The threshold voltage was determined from the intercept of the fitting line used to extract the mobility in the linear regime ($I_D$- $V_{GS}$ characterization) as shown in the Figure 25 or the intercept of the fitting line used to extract the mobility in the saturation regime ($\sqrt{I_D}$-$V_{GS}$ characteristics). Although the threshold voltage is mostly dominated by the properties of the gate dielectric and the dielectric/polymer interface, we observe a small dependence on the modified source and drain electrodes, even though no clear trend is observed.

#### 2.4.1.2 Modified transfer line method (M-TLM)

We can look more precise into the TLM method which is used to calculate mobility and contact resistance. In the field-effect transistor, the bottom gate induces charges (holes in our case) into the channel, which does not depend on the contact. Therefore, whether the electrodes are modified with SAM or not, the channel resistance should be the same as long as devices with exactly the same geometry are investigated. From the formula (7), $R_C$ for SAM treated devices can be calculated:

$$R_C(SAM) = R_{ON} - R_{Ch}(SAM) \times L \qquad (11)$$

If the above assumption is correct $[R_{Ch}(SAM) = R_{Ch}(NoSAM)]$, then we can use the date of $R_{ch}$ for untreated transistor in the above formula:

$$R_C(SAM) = R_{ON} - R_{Ch}(NoSAM) \times L \qquad (12)$$

We believe this modified-TLM method is more precise for calculating the contact resistance of the SAM-treated transistors. To check this assumption, series of ring transistors with channel length from 10, 15, 20, 30 and 40 µm and width of 1000 µm are measured with untreated and HDT-treated electrodes. Figure 28(a) shows that the $R_{ch}$ calculate from TLM method and with modified TLM (M-TLM) especially in the higher gate voltage are the same.

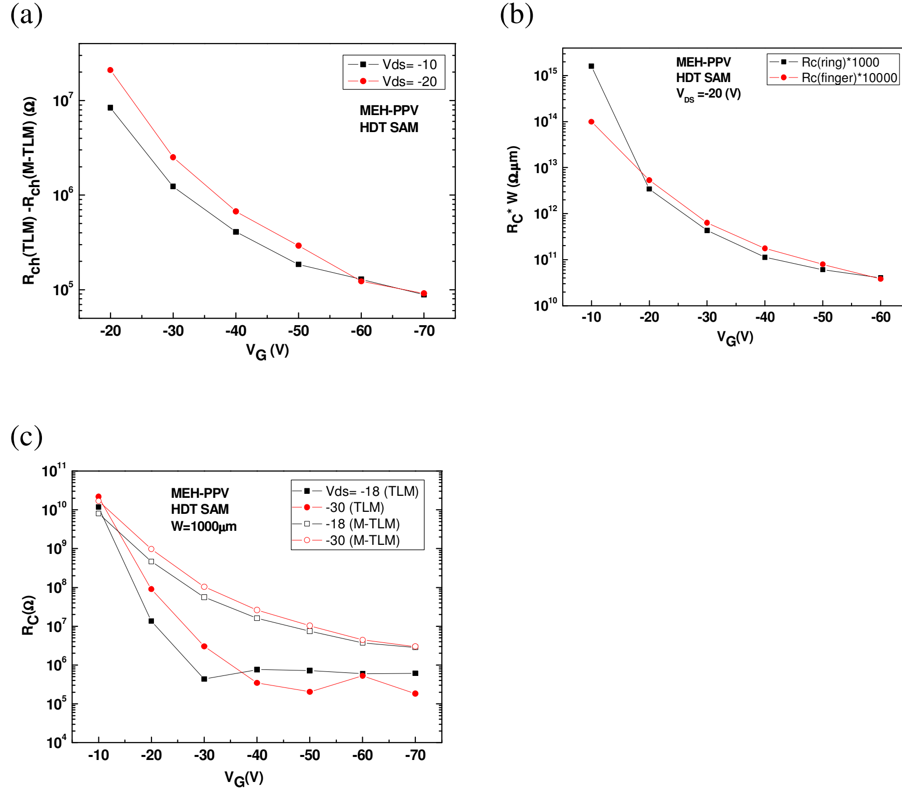


**Fig. 28** (a) Channel resistance versus gate voltage are similar in the TLM and M-TLM analysis. (b) Contact resistance in HDT-modified electrodes with TLM and M-TLM for different $V_{DS}$. (c) Contact resistance in finger and ring transistors with M-TLM are identical within the error margins.

Now, we calculate contact resistance of the HDT-modified transistors with M-TLM analysis and compare with the TLM one. As shown in Figure 28(b), $R_C$ for two $V_{DS}$ in the M-TLM are same with a better trend as compared to the TLM analysis. In general in the ring transistors field is better defined than the finger transistors, since all field lines are perpendicular to the electrodes. However, the width in our ring transistor was 1000 µm which lowers the current compare to the fingers with widths of 10000 µm and also high leakage current is observed. However in this case, the $R_c$ in both geometry for the same channel length of transistors calculated by M-TLM is the same (Figure 28(c)).

### 2.4.2 rr-P3HT

Regioregular poly(3-hexyl thiophene) (rr-P3HT) has been the subject of many studies in OFETs (Figure 29). Due to presence of highly ordered crystalline phases at the semiconductor/dielectric interface, a higher mobility is obtained compared to other semiconducting polymers.

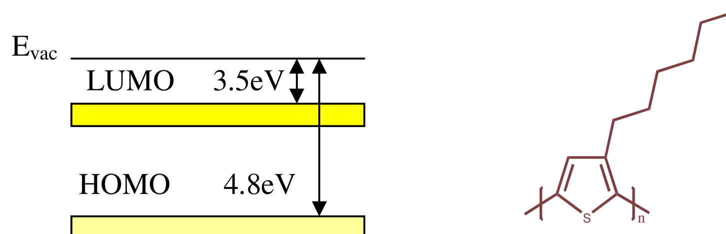


**Fig. 29** HOMO and LUMO of rr-P3HT, and the chemical structure of that polymer.

We have studied charge injection across the metal/ rr-P3HT interface in BC/BG field-effect transistors with Au source and drain electrodes, which are modified by SAMs. The output characteristics of untreated and HDT-modified finger transistors with L/W=20/10000 are shown in Figure 30(a). Mobility and contact resistance calculated by TLM for a series of finger transistors with channel width of 10000 μm and channel lengths of 10, 15, 20, 30 and 40 μm shown in Figure 30(b) and 30(c). Since the HOMO level of rr-P3HT is located at 4.8 eV, an Ohmic contact is created with Au electrodes. For HDT treated Au contacts, the work function is changed to ~4.0 eV. Consequently, an injection barrier for holes is expected, although this blocking is smaller than for MEH-PPV, it is still present. The mobility calculated for both transistors characteristics (untreated and HDT-treated) is $1–2\times10^{-2}$ $cm^2$ $V^{-1}$ $S^{-1}$ at $V_{DS}$= –2V and high $V_G$, which is similar to the reported mobility for rr-P3HT. The contact resistance for the SAM-modified Au electrodes is one order of magnitude larger than the transistor with bare Au electrodes which can be attributed to the increase of the injection barrier due to presence of the insulating monolayer between the Au electrode and polymer. This is valid if we assume that rr-P3HT adopts the same morphology at the interface with the Au electrode in the presence or absence of the SAM. We measure all the experiments with rr-P3HT at room temperature without any thermal treatment. Although the on/off ratio of the transistor is increased upon annealing while the mobility remains constant

but in the case of using SAM-modified electrodes, one has to be careful using temperature treatment of the transistors since SAMs of alkanethiol are thermally unstable at temperature above 70°C. Furthermore, annealing will influence the anisotropic nature of the charge transport in rr-P3HT. [25]

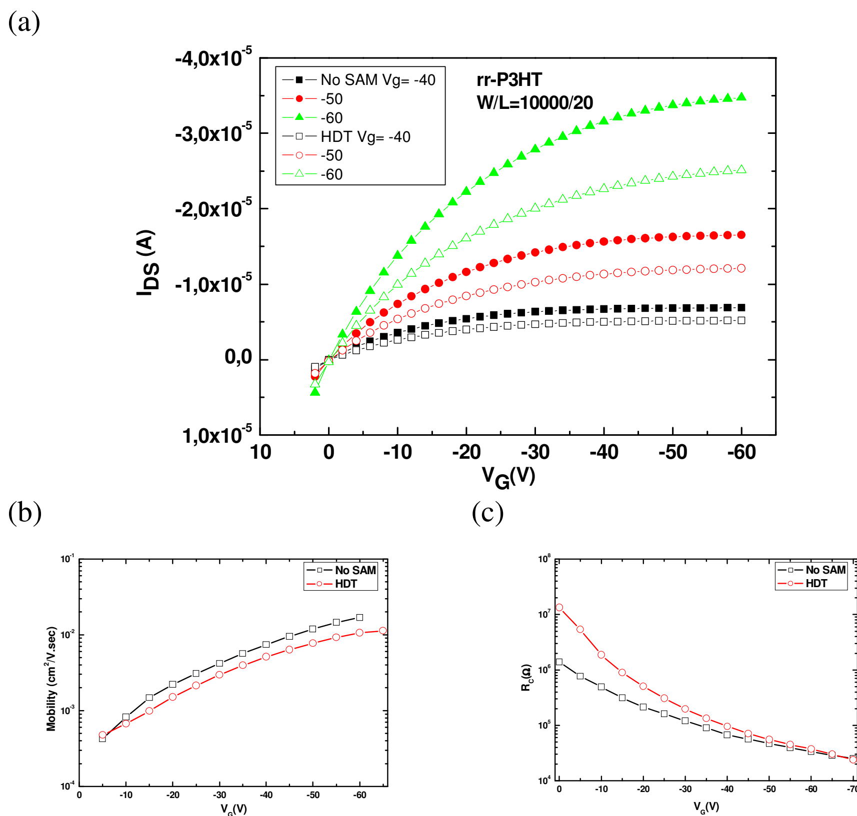


**Fig. 30** (a) The output characteristics of HDT modified and unmodified Au electrodes in rr-P3HT transistors. (b) Comparison of the mobility and (c) Contact resistance at $V_{DS}$= -2 V.

The presence of a perfluorinated SAM (PFDT) with $CF_3$ end groups drastically alters the surface energy and this SAM results in a highly hydrophobic surface, which causes a poor wetting of the rr-P3HT on the contacts. Therefore, we omitted data based on PFDT-modified transistors. Similar arguments on hydrophobicity hold for Au electrodes with HDT SAMs. However, the current-voltage characteristics of untreated transistors

and transistors with HDT-modified gold electrodes are reliable and reproducible.

To investigate more precisely the effect of the length of alkanethiols SAMs on charge injection and therefore contact resistance of OFETs, various alkanethiols are used to modify gold electrodes. First undecanethiol (UDT; $C_{11}H_{23}$-SH) and hexadecanethiol (HDT; $C_{16}H_{37}$-SH) SAMs are applied in the OFET structure using rr-P3Ht as the semiconductor. The output characteristic are compared with the untreated electrodes in Figure 31 for finger transistors with W/L=10000/20.

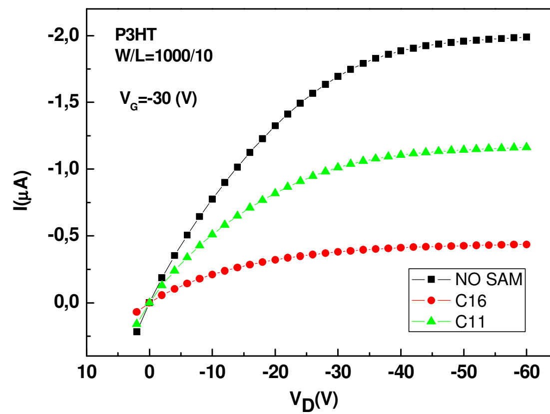


**Fig. 31** The output characteristic of HDT and UDT modified electrodes compared with unmodified electrodes in rr-P3HT based transistors.

In the output characteristic, we can see that the current for untreated electrodes is higher than those treated with the two alkanethiols SAMs. These SAMs are expected to block the current, but the UDT has shorter length so it has weaker effect compare to the HDT one

In the other experiment, SAM molecules of the butanethiol ($C_4H_9$-SH), Nonanethiol ($C_9H_{19}$-SH) and Decanethiol ($C_{10}H_{21}$-SH) were also used. To see the effect of the contacts better, transistors with small length were measured. Figure 33 shows the contact resistance for finger transistors by various lengths: 0.75, 1, 1.5, 1.75, 2.5, 5 and 7.5 µm and width 10000 µm (Figure 32).

Since SAM molecules can introduce an injection barrier as well as an insulating barrier at the interface, increasing the length we expect an increase of the contact resistance because the width of the tunnel barrier for injection of charge carrier is increased at the interface. A trend can be

observed from $C_4$ to $C_{11}$ in comparison with unmodified electrodes. $C_{16}$ does not follow the trend, which can be due to some unknown external factor during the preparation of the samples; however, the experiment should be repeated.

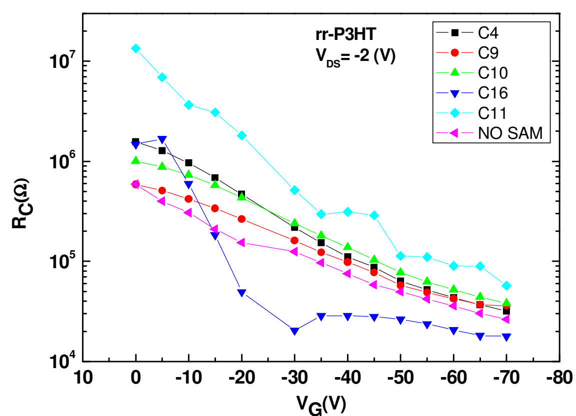


**Fig. 32** Contact resistances of different alkanethiols SAM calculated by TLM.

## 2-4-3 PFO

Poly(9,9-dioctylfluorene) (PFO), shown in Figure 33, is an amorphous polymer with wide band gap, which is mostly used as the blue light-emitting material in the PLED structure. PFO exhibits its HOMO and LUMO level of ~5.9 eV and 2.6 eV, respectively.

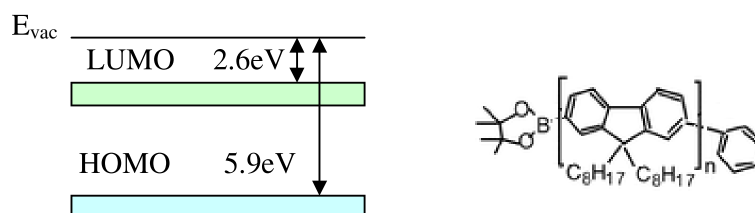


**Fig. 33** HOMO and LUMO of PFO and its chemical structure.

Therefore if this material is used in the FET devices with gold electrodes, there will be an injection barrier of ~1 eV for the holes to be injected into the HOMO of PFO. Consequently, the output current is expected to show a very low current and the output characteristics decrease further by using a SAM of HDT which decreases the work function of gold contacts to 4.0 eV. However, with the PFDT SAM the work function of the gold electrode increases to ~5.6 eV and the field-effect behavior of PFO should be amplified.

Three sets of transistor were measured, PFDT and HDT modified as well as unmodified transistors as the reference device. For PFDT modified, a lower injection barrier is expected, and indeed the field-effect is observed in the PFO/ PFDT/ Au transistors. However, the result for the unmodified transistors was unexpected. Because of the high injection barriers in the case of PFO/Au, no field-effect behavior was expected but devices showed high current! Figure 34 shows the output characteristics of such a device for finger transistors with W/L=10000/40 µm. Although the gate voltage can increase to higher values and the amount of induced charges becomes enough to lower the barrier to some extent and that makes it possible for the hole to be injected from the electrode. This experiment was repeated three times, and the result was the same! From theoretical point of view this result is not  quiet correct and was out of expectation.

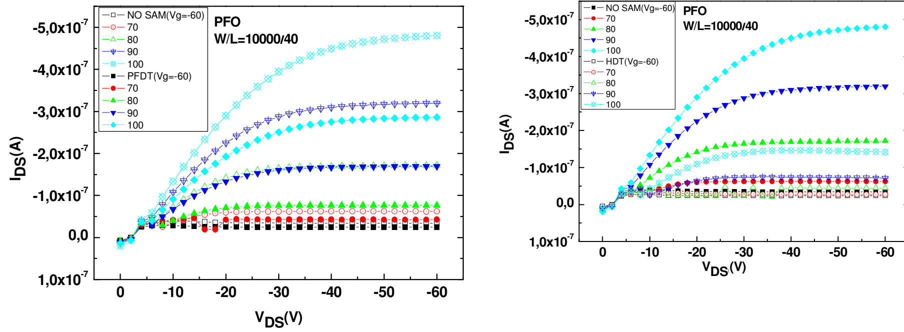


**Fig. 34** The output characteristics for SAM-modified in comparison with unmodified electrodes in PFO-based transistors.

The transfer characteristic of the transistor in the linear regime ($V_{DS}$= -10 V) is shown in Figure 35(a) and saturation in (b), which reveals that the transistor switches on at very high gate voltages.

(a) (b)

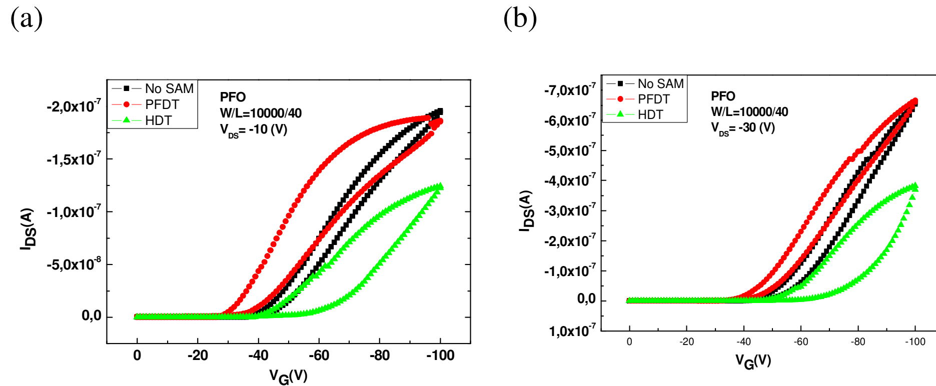


**Fig. 35** (a), (b) Transfer characteristics in linear ($V_{DS}$= -10V) and saturation ($V_{DS}$= -30V) regime.

From the data, the mobility and the contact resistance for a series of the transistors with the W=10000 µm and different length from 7.5 to 40 µm were calculated by the TLM method. The results for the saturation regime are given in Figures 36(a) and (b). The same value was obtained for PFDT and HDT modified devices as well as the unmodified devices, which again shows the mobility is the material properties and does not depend on the contact. The mobility is about $10^{-4}$ $cm^2$/V.sec.

(a) (b)

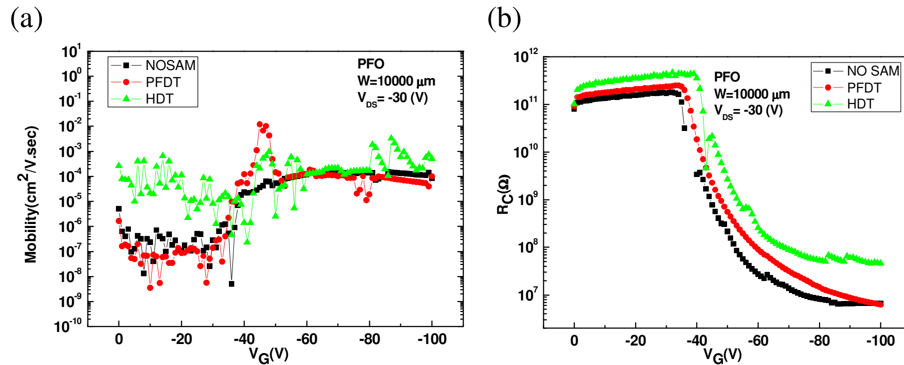


**Fig. 36** (a) The mobility and (b) Contact resistance for PFO based transistors without gold electrode and with gold electrodes modified by PDFT and HDT.

The contact resistance clearly shows threshold voltages up to -40 V at which the transistors is turned on, and by increasing the gate voltage the resistance will be decreased which means that the FETs made from PFO work only at very high gate field. If working transistors with PFO and modified contacts are required that operate at lower gate voltages, the contacts should be modified with the molecules with larger dipole.
The contact resistance graph also shows the effect of the SAM on the contacts, for HDT the resistance is higher due to the longer alkane chain, while for PFDT and pristine devices is lower.

# Chapter 3
# Experiment (Part 2)

In BC/BG transistors, charges are injected from the edge of the electrodes and mainly closed to the semiconductor/dielectric interface. The molecular monolayer on the electrodes in this case is very ill-defined due to the ill-defined Au surface. However, in the BC/TG geometry, SAM molecules are situated on top of the surface of the primarily Au(111) surface. SAMs on Au (111) are very well characterized. Due to the larger effective contact area (overlapping of the top gate and the contacts) between the semiconductor and the electrodes, the injection is improved and mimics that of a diode. Therefore, BC/TG transistors were processed and the effect of the SAM on the charge injection, in this geometry, investigated.

To clean the surface and remove moisture, 4 or 6 inch prime grade silicon wafer cleaned with acetone and 2-propanol, and dried by a deionized $N_2$ flow. The adhesion promoter hexamethyldisilazane (HMDS) is drop casted on the substrate to enhance the wetting of the photoresist on the wafer. The residual of HMDS is removed by acetone and 2-propanol and dried through spinning. Negative photoresist (Ma-N1410) is diluted with photoresist thinner (Ma-T1046) in a 1:7 ratio and left on a stirring plate for some hours. Spin coating the photoresist is done outside of the glove box. Substrates are backed at 95°C on a hotplate for 90 seconds. This step hardens the photoresist slightly and remove solvents. The backing times depends on the thickness of the photoresist. After photolithography, the substrates are kept for 45 seconds in the developer (ma-D533 S) and 1 min in the ultra pure water flow (18 MΩ) and dried on the spinner. The speed and acceleration with which the photoresist is applied will determine its thickness. Layer thicknesses were determined using a Dektak profilometer.

## 3.1 Photolithography

Photolithography, literally meaning *light-stone-writing* in Greek, is the process by which patterns on a semiconductor material can be defined

using light. Before the resist is applied to the substrate, the surface is cleaned to remove any traces of contamination such as dust, organic, ionic, and metallic compounds. A resist is applied to the surface using a spin coating machine. This device holds the wafer of semiconductor, using a vacuum, and spins it at high-speed (3000 or 6000 rpm) for a period of 15-30 seconds. Preparation of the resist is concluded by a pre-bake, where the wafer is heated on the hotplate to evaporate the resist solvent and to partially solidify the resist. Alignment of the photo mask is critical step.[29]

The action of light on a positive resist causes it to polymerize where it has been exposed to the light. The duration of the exposure is depending on the thickness of the photoresist, which can vary between 5-30 seconds.

### 3.2 Thermal Evaporation

The evaporation of metals is done in the deposition system in the glove box. Thermal evaporation is the simplest method. This process is usually carried out in a bell jar with a pressure less than $10^{-6}$ mbar. A tungsten boat is heated up by its resistance while very high electrical current passes through. As the temperature rises, the metal to be deposited is melted and wets the boat. The current through the filament is increased further, until the metal vaporizes. The metal vapor then condenses on the cooler surface of the semiconductor, forming the desired pattern of the metal layer.

After developing the photoresist, the substrates are transferred to the evaporation glove box. An interlayer of Cr of 1-2 nm thick was evaporated first for the better adhesionafter which gold was evaporated. The gold layer is 40-50 nm thick. The lift off step to remove the photoresist on the substrate is carried out for 20 min in ultrasonic bath by submerging the wafer in acetone. The substrate is rinsed by 2-propanol and dried. After cutting the wafer into small pieces (3cm×3cm), cleaning with acetone and 2-propanol, the substrates were subjected to UV-Ozone cleaning (for the removal of organic remains) for 5-20 minutes. A Piranha solution (Demi water 100ml + ammonia (30 %) 20 ml + $H_2O_2$ 20 ml) was used for 45 s at 70 ºC to remove all organic impurities on the Au electrodes. Subsequently, the substrate is submerged in the SAM solution or pure ethanol over night. After SAM deposition the substrates were treated by rinsing as explained in part I. Before spin coating in the nitrogen glove box, HMDS is applied and the substrates were washed to remove residual HMDS. 4 mg/ml MEH-PPV was

spin coated using the spin program listed below. The layer thickness is around 40-50 nm.

| | Speed (rpm) | Acceleration (rpm/s) | Time (second) |
|---|---|---|---|
| 1- Open | 1500 | 5000 | 5 |
| 2- Close | 300 | 500 | 60 |

After spin coating of the semiconducting polymer, an organic gate dielectric is applied by spin coated a 40 mg/ml poly(trifluoro ethylene) (PTrFE) solution in methyl ethyl ketone (MEK). PTrFE is a polymeric insulator with a dielectric constant around 10 and is used as a top gate dielectric. The thickness obtained with program listed below is around 300-400 nm.

| | Speed (rpm) | Acceleration (rpm/s) | Time (second) |
|---|---|---|---|
| 1- Open | 1000 | 5000 | 30 |

Finally, the transistors were transferred to the evaporation system to evaporate 80 nm gold or silver top gate electrode by using a shadow mask. (Figure 37)

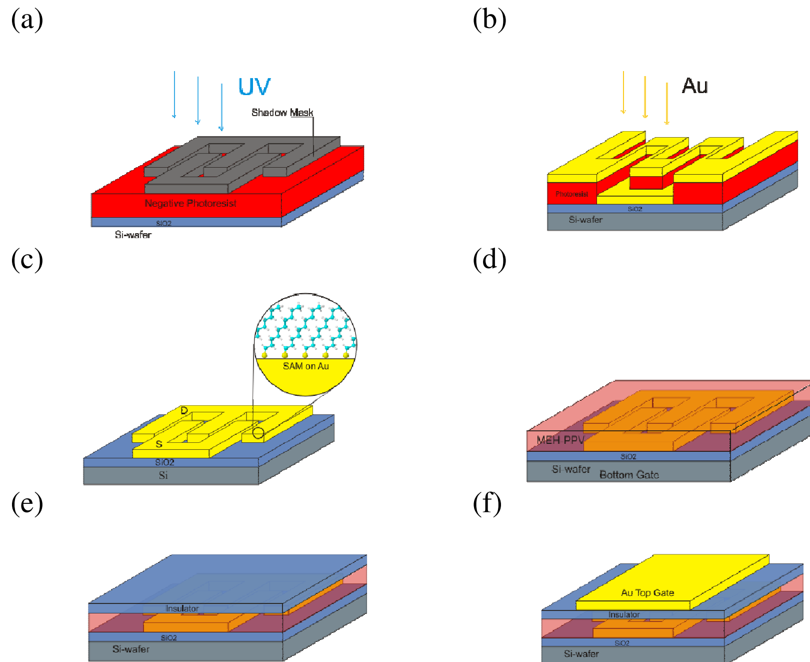


**Fig. 37** Steps of making a dual gate OFET.

## 3.3 Results and Discussion (Part 2)

Dual gate polymeric field-effect transistors were made with gold source and drain electrodes and a gold top electrode as a gate. Thickness of the $SiO_2$ bottom gate dielectric (ε=3.9) is 500 nm and the thickness of PTrFE with (ε= 10) is determined to be around 250 nm.

The output characteristic and transfer characteristics in the saturation regime for finger transistor with a width of 1 mm and the channel length of 10 µm in BC/BG and BC/TG configuration are shown in Figure 38.

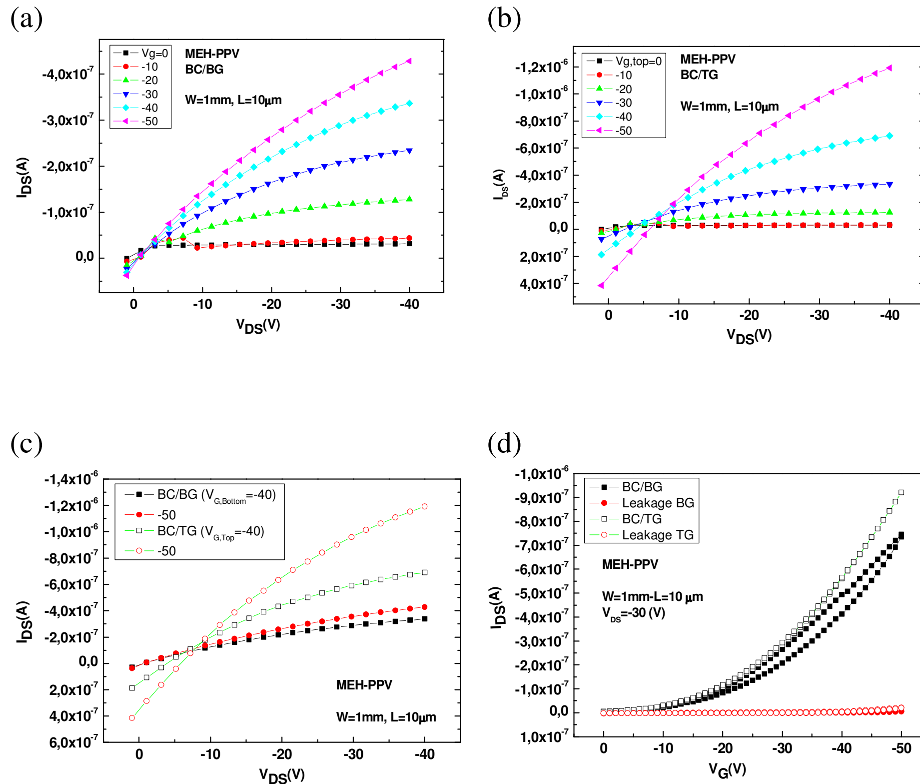


**Fig. 38** (a), (b) The output characteristics in BC/BG and BC/TG geometry with gold source, drain and top gate electrodes, (c) comparison of the current in these two geometries and (d) the transfer characteristic in both configuration at $V_{DS}$= -30V. The $V_{G,Bottom}$ and $V_{G,Top}$ is indicated by $V_G$ in this figure.

From the comparison of the output characteristic in the higher gate voltage regime for these two geometries, Figure 38(c), it is clear that BC/TG devices showed better performance with higher currents than BC/BG devices on the same semiconductor layer. In general, transfer characteristics are affected by hysteresis; in particular the hysteresis is almost negligible in BC/TG devices, while it is most pronounced in BC/BG geometry as is shown in Figure 38(d). The mobility and contact resistance calculated by the TLM method for a series of transistors with channel width of 2 mm and channel lengths of 5, 10 and 20 μm in the saturation regime are shown in Figure 39.

The contact resistance is much lower in the BC/TG devices, meaning that the charge injection between metal/semiconductor is favored in this kind of structure. The interface between the electrode and the semiconductor layer is much larger and much more uniform for BC/TG devices than for BC/BG FETs. Thus the contact resistance is reduced as supported by the data.

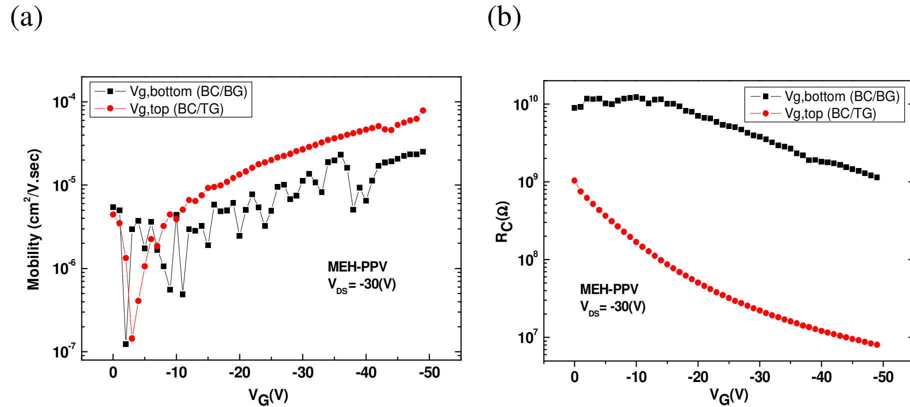


**Fig. 39** (a) Mobility and (b) Contact resistance as determined via TLM for a comparison between BC/BG and BC/TG.

The two geometrical structures have similar channel characteristics and, consequently, should have similar mobility values. However, a small difference is calculated for the mobility. In the case of BC/TG devices, the recorded field effect motilities are higher that the ones measured in BC/BG devices. Besides the difference in the source and drain contact geometry as explained above, both BC/TG and BC/BG have exactly the same source and

drain electrode and the same semiconductor. Therefore, the difference in motilities can be attributed to the difference of the dielectric insulating film. In the case of BC/BG devices, the dielectric interface can lead to an increase in the interface trap states compared to BC/TG structures. This can be the reason for the increase in the series contact resistance, the lower mobility and the larger hysteresis of the recorded electrical characteristics for the BC/BG devices. These characteristics are directly reflected in the performance of the reported devices and, consequently, the BC/TG transistors perform better than BC/BG FETs. The field effect mobility extracted from the saturation regime is not affected by contact resistance. We believed that this is because of the favorable influence of the applied gate field aiding injection in a BC/TG geometry. Charge injection does not only occur at the edge of the electrodes, but over a larger area away from the edge because of the overlap of the gate electrode and the source and drain electrodes.

In this part, the results of the dual gate OFETs are shown with gold source- drain and a silver top gate electrode. Thickness of the $SiO_2$ bottom gate dielectric is 1000 nm and the thickness of PTrFE top gate dielectric is around 300 nm.

In the previous experiment lots of transistors were short circuited especially for HDT SAM modified transistors, in which all devices were short circuited. Diffusion of the vapor-deposited gold top gate into polymer layer can be the reason, and therefore silver is used as a top gate electrode because silver is expected to diffuse less than gold.

The stable OFET operation requires the gate leakage current to be around $10^{-9}$A. The leakage current and large hysteresis in the BC/BG geometry can relate to damage of the $SiO_2$ during the cutting process, or film morphology in the bottom channel. This time, to solve leakage current problem, and to have better performance in dual gate transistors, the cleaning process was improved by using one step cleaning in Piranha solution. Prime grade silicon wafer are used because the wafers are more easily cut, which, at the end, helps to precisely align the substrate during the vapor-deposition of the top gate electrode. Furthermore, the optimization of the exposure time in photolithography step helped improving the devices. The output characteristic is shown in Figure 40. The conclusion is same as in the previous experiments, except that none of the devices were not short circuited.

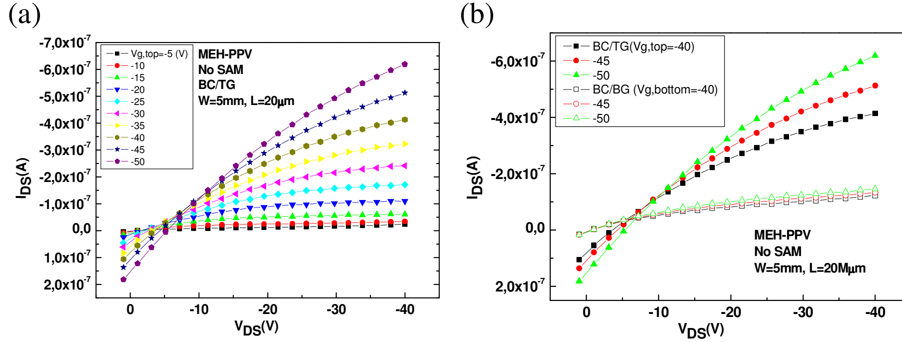


**Fig. 40** (a) The output characteristics in BC/TG with gold source and drain electrodes and silver top gate electrodes with MEH-PPV polymer, (b) The comparison of the current in these two geometries.

The mobility and contact resistance for a series of transistor with width of 5 mm and channel lengths of 5, 10 and 20 μm are calculated using TLM and depicted in Figure 41. The results again show lower contact resistance and higher mobility for the top gate configuration. The top gate configuration is generally less sensitive to contact resistance than bottom gates ones, because the effective area of the contact is larger due to overlap of the gate and source-drain electrodes.

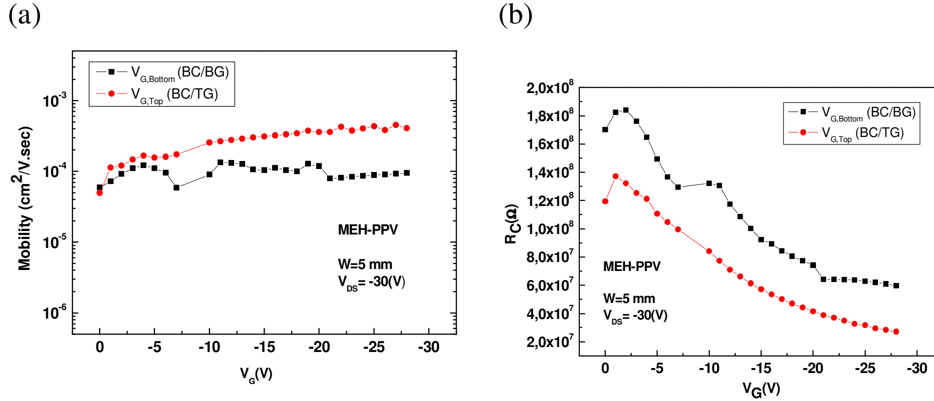


**Fig. 41** (a) Mobility and (b) contact resistance for MEH-PPV based dual gate FETs as calculated via the TLM method.

After we found the best way to make dual gate polymeric FETs, SAMs of HDT and PFDT are also applied to see the effect of the SAMs in

the top gate geometry and to compare the characteristics with the bottom gate configuration. Gold source- drain electrodes and a silver top gate electrode are used. Thickness of the $SiO_2$ bottom gate dielectric is 1000 nm and the thickness of PTrFE top gate dielectric is around 450 nm. Thickness of top gate dielectric is crucial; by increasing this thickness we can prevent diffusion of the vapor-deposited metal atoms of the top gate in to the polymer layer. The output characteristics are shown in comparison with the untreated transistor.

(a) (b)

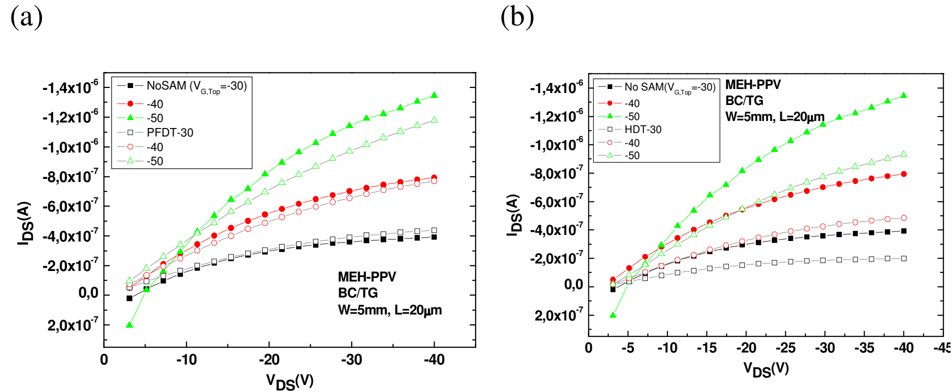


**Fig. 42** The output characteristic for HDT (a) and PFDT (b) modified gold electrodes in the MEH-PPV based top gate transistors.

Now we have shown that reproducible dual gate device are made with a silver top gate electrode and gold source and drain electrodes and that we can modify the source and drain electrodes with HDT and PFDT SAMs. The obvious next step, using the same structure, is to apply silver source and drain electrodes with a silver top gate. Up to now gold was used as a stable metal, however, using PFDT does not improve the hole injection since Au already provides an ohmic contact and only HDT modifies the injection by blocking the hole injection from gold electrodes into MEH-PPV. However, one of the aims of using SAMs is to improve the charge injection of metal electrodes, thus silver can be a good option. The work function of the silver is ~ 4.3 eV which makes this metal an injection limited contact creating an injection barrier of around 1 eV with MEH-PPV. Using an HDT SAM on Ag decreased the work function of silver to 3.8 eV which really blocks the hole injection, but PFDT increases the work function to 5.5 eV which completely eliminates the injection barrier and makes an ohmic contact. So injection of holes into the HOMO of the MEH-

PPV will be improved using a PFDT SAM on Ag as compared to the bare silver source and drain electrode. Before using a SAM, the BC/BG field-effect transistor with bare silver electrodes is prepared to investigate the characteristics of the reference devices, because silver is very sensitive to oxygen and make silver oxide quickly. Thickness of the $SiO_2$ gate dielectric is 250 nm. The output characteristic is shown in Figure 43 for a transistor with width of 2 mm and a length of 5 μm. As one can see, a non-linear behavior of the output characteristic clearly indicates the existence of an injection barrier between silver and MEH-PPV.

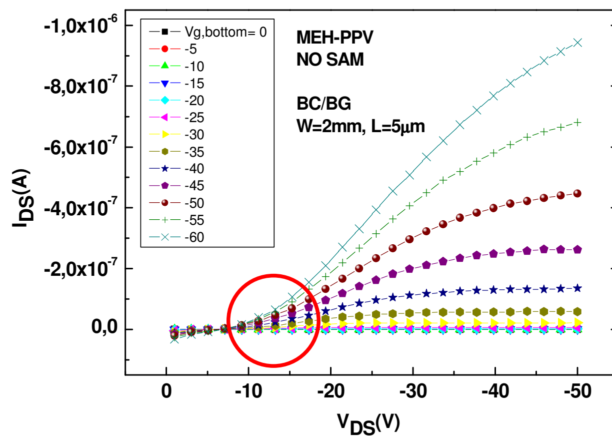


**Fig. 43** The output characteristic for unmodified silver source and drain electrodes in BC/BG configuration.

Subsequently, 500 nm PTrFE is spin coated on top of MEH-PPV followed by the evaporation of an Ag top gate electrode. The output curves are shown in Figure 44 for a transistor with a width of 2 mm and a channel length of 5 μm. The result for mobility is shown in Figure 45. The top gate mobility is higher by one order of magnitude compared to the mobility calculated for the bottom gate channel. Furthermore, devices were fabricated with silver source and drain electrodes which are treated with the HDT SAM to increase the injection barrier. All transistors with HDT SAM were short circuited! This can be due to the de-wetting of the polymer on the surface, or remains of silver in the channel after lift off.

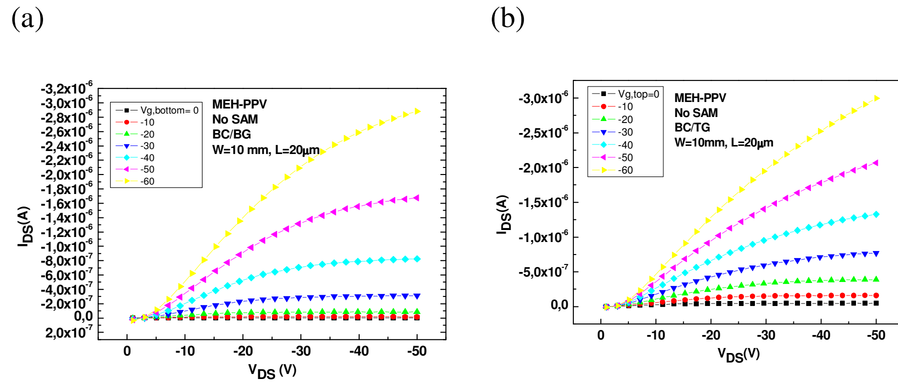


**Fig. 44** (a), (b) The output characteristic for unmodified silver source and drain electrodes in the MEH-PPV based transistors in BC/TG and in BC/TG geometry for different gate voltages.

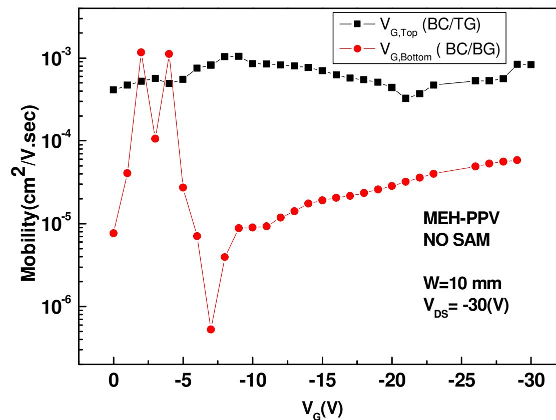


**Fig. 45** Mobility calculated using TLM for unmodified silver electrodes in the BC/BG and BC/TG configuration.

The experiments were repeated again in a more precise way. Again silver source and drain electrodes and a 80 nm top gate electrode were evaporated and complete dual gate transistors were produced. Thickness of the $SiO_2$ bottom gate dielectric is 250 nm and thickness of the PTrFE top dielectric layer is around 400 nm. 40-50 nm MEH-PPV (4 mg/ml) was spin-coated as semiconductor. PFDT and HDT modified silver electrodes were measured. The output characteristics of the modified silver electrodes are compared to the untreated electrodes and are shown in Figure 46, for transistors with a

width of 20 mm and a channel length of 20 µm. The TLM-mobility shows that BC/TG has a higher mobility compared to BC/BG.

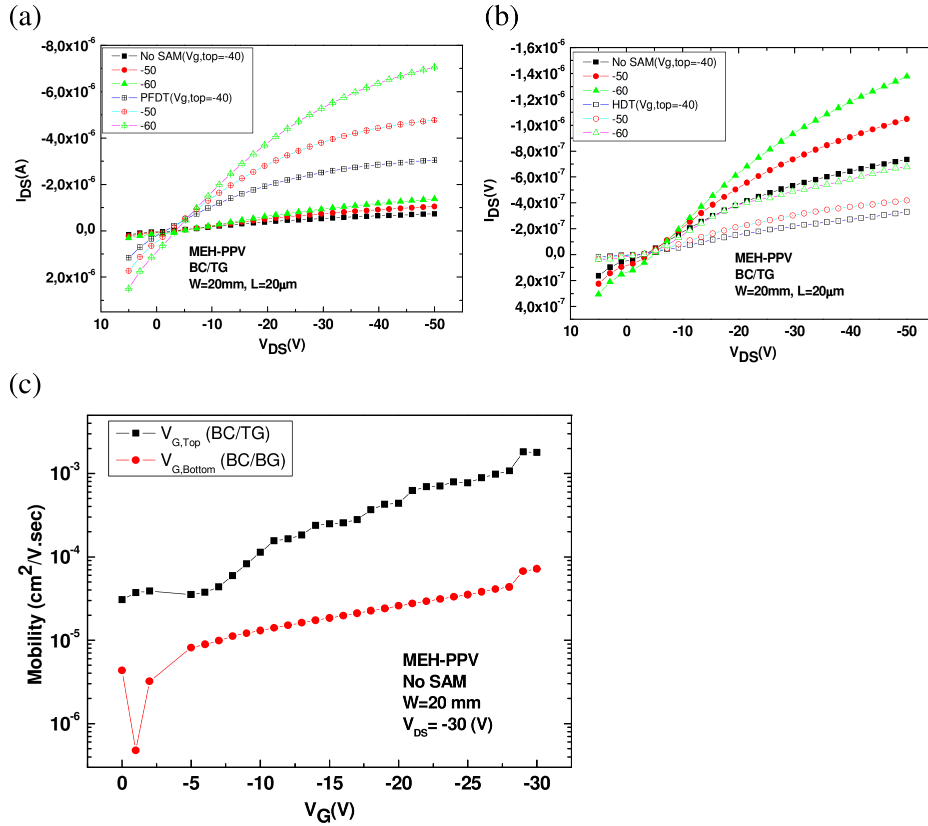


**Fig. 46** The output characteristic for bare silver electrodes and for silver electrodes modified by PFDT (a) and HDT (b) in BC/TG geometry and (c) the mobility calculated by TLM for untreated silver contacts in BC/TG and BC/BG geometry.

# Conclusion

We demonstrate by using self-assembled monolayers in organic field-effect transistors, that the work function of the gold or silver electrodes can be modified. The charge injection can be improved or blocked by using different SAMs with opposing dipoles. Using the transfer line method (TLM), we have found the intrinsic mobility for MEH-PPV ($4\times10^{-3}$ $cm^2V^{-1}s^{-1}$) and rr-P3HT ($1–2\times10^{-2}$ $cm^2V^{-1}s^{-1}$) to be irrespective of the contacts. The contact resistances extracted from the TLM are larger for the SAM-modified gold contacts with respect to the untreated electrodes in case of these two polymers. Consequently, the field-effect behavior of PFO in transistors with gold contact and with SAM-modified electrodes could be measured. Its field-effect mobility was calculated and resulting in $1\times10^{-4}$ $cm^2V^{-1}s^{-1}$.

Also the effect of the SAMs is investigated in the bottom source-drain contact (BC)/ top gate (TG) geometry. The BC/TG devices often have improved device performance when compared to the performance of devices with photolithographically defined bottom contacts/bottom gate (BC/BG). We expect that the surface roughness and the presence of an oxide or self-assembled molecular layer strongly influence the film morphology on the metal and along the contact edge, which affects the charge injection and the transport near the contact. For a top gate configuration the key parameter is the choice of insulator material (and solvent) while for the bottom gate configuration, device performance is largely dependent on interfacial properties, which may be controlled by, for example, surface treatments. Also the mobility calculated by TLM shows higher value in BC/TG and lower contact resistance compared to BC/BG.

# Out Look

The following research can be done for future work to investigate the effect of SAMs in FETs geometries.

1- Using different type of organic self-assembling molecules with different electric dipoles to tune the work function. Particularly, conjugated SAM can be used as a semiconducting SAM to facilitate the injection of charge carriers.
2- Modifying the source and drain electrodes with two different SAMs at the same time, to block the injection of holes from the source, and enhance the electron injection from the drain.
3- Using different top gate dielectric to reduce the roughness and facilitate the transport of holes or electrons in the channel.
4- Using other polymers also in the BC/TG geometry.
5- Repeating the measurements with PFO polymer in the BC/BG and in BC/TG.

# Acknowledgment

I thank Prof Paul Blom for accepting me in his group and his guidance during my master project. I'm also very grateful to Bert de Boer for supervising me and very special thanks for Kamal Asadi who was my daily supervisor during this year, and helped me with many problems that I had at the beginning of my research. I also thank in particular Afshin, Hylke, Oleksandr, Auke, Johan, Milo, Francesco, Maria, our technicians Frans, Jurjen and special thanks to Jan Harkema for his invaluable technical help and assistance and other people in the group of Molecular Electronics: Physics of Organic Semiconductors.

# References


1 http://nobelprize.org/educational_games/physics/transistor/history/
2 J. E.Lilienfeld, *US patent* 1745175 (1930).
3 D. Kahng, M. M. Atalla, *IRE Solid-State Devices Research Conference*, Carnegie Institute of Technology, Pittsburgh, PA (1960)
4 G. Horowitz, *Adv. Mater,* 10, 5 (1998)
5 H. Koezuka, A. Tsumura, T. Ando, *Synth Met,* 18, 699 (1987)
6 P. Cosseddu, A. Bonfiglio, *Elsevier*, 22475, 5 (2007)
7 D. Natali, L. Fumagalli, M. Sampietro, *J. Appl.Phys.* 101, 014501 (2007)
8 B. de Boer, A. Hadipour, M. M. Mandoc, T. Woudenbergh, P. W. M. Blom, *Adv. Mater.* 17, 5 (2005)
9 B. de Boer, Opto-Electronic Properties of Polymer, lecture notes, University of Groningen (2004)
10 F. Gholamrezaie, Do molecular rectifier exists?, review paper, University of Groningen (2006)
11 K. Asadi, Master thesis, Using SAM in FETs, University of Groningen (2005)
12 E. Meijer, Charge Transport in Disordered Organic Field Effect Transistors, Phd thesis, Delft University of Technology (2003)
13 J. Zaumseil, H. Sirringhaus, *Chem. Rev.* 27, 1 (2007)
14 E. J. Meijer, G. H. Gelinck, E. Van Veenendaal, B. H. Huisman, D. M. de. Leeuw, T. M. Klapwijk, *Appl. Phys. Lett*. 82, 25 (2003)
15 Th. Singh, N. S. Sariciftci, Annu. *Rev. Mater.* 36, 199, (2006)
16 G. Horowitz, P. Lang, M. Mottaghi, H. Aubin, *Adv. Funct. Mater. 14*, 11(2004)
17 S. M. Sze, Physics of Semiconductor Devices, John Wiley, USA (1981).
18 Y. Shen, A. R. Hosseini, M. H. Wong, G. G. Malliaras, *ChemPhysChem*, 5,16 (2004)
19 G. Horowitz, R. Hajlaoui, D. Fichou, A. El Kassmi, *J. Appl. Phys.* 85,3202 (1999)
20 L. Burgi, T. J. Richards, R. H. Friend, H. Sirringhaus, *J. Appl. Phys*. 94, 6129 (2003)

21 E. J. Meijer, C. Tanaze, P.W.M. Blom, E, Veenendaal, B. Huisman, D. M. de Leeuw, T. M. Klapwijk, *Appl .Phys. Lett.* 80, 3838 (2002)
22 M. J. Deen, F. Pascal, *J. Mater Sci.* 17, 549 (2006)
23 A. Facchetti, M. Yoon, T. J. Marks, *Adv. Mater.*17, 1705 (2005)
24 S. Kobayashi, T. Nishkawa, T. Takenobu, S. Mori, T. Shimoda, T.Mitani, H. Shimotani, N. Yoshimoto, S.Ogawa and Y.Iwasa, *Nat. Mater.* 3, 317 (2004 )
25 K. Asadi, F. Gholamrezaie, E. C. P. Smit, P. W. M. Blom, B. de Boer, *J. Mater Chem.* 17, 1947 (2007)
26 P. C. Rusu and G. Brocks, *J. Phys. Chem.* 74, 073414 (2006)
27 H. B. Akkerman, R. C. G. Naber, B. Jongbloed, P. A. van Hal, P. W. M. Blom, D. M. de Leeuw, and B. de Boer, Proc. *Natl. Acad Sci. (PNAS)*, 104, 11161 (2007)
28 K. P. Pernstich, S. Haas, D. Oberhoff, C. Goldmann, D. J. Gundlach, B. Batlogg, *J. Appl.Phys.* 96, 11 (2004)
29 http://en.wikipedia.org/wiki